



**GEOMAR Helmholtz Centre for Ocean Research Kiel**

Forschungsbereich 4: Dynamik des Ozeanbodens  
FE Marine Geodynamik  
Wischhofstraße 1-3  
D-24148 Kiel, Germany

Telephone: +49 431 600-2556, Email: [brad.weymer@gmail.com](mailto:brad.weymer@gmail.com)

Bradley A. Weymer  
GEOMAR Helmholtz Centre for  
Ocean Research Kiel  
Wischhofstraße 1-3  
D-24148 Kiel  
Germany

April 22, 2018

Please find below our point-by-point responses and explanations for how we addressed the comments by the Reviewers on the earlier version of this manuscript.

**REVIEWER #1:**

Thank-you for the opportunity to review the manuscript “Statistical modeling of the long-range dependence structure of barrier island framework geology and surface geomorphology” by Weymer, et al. The writing style of this contribution is excellent, the authors should be commended. The manuscript for the most part is clear, coherent and well organized. The research utilizes Electromagnetic Induction (EMI) and GPR data, and topography, to examine the long-range dependence of the framework geology and the geomorphology of Padre Island in the Gulf of Mexico, and interpret the results of ARIMA statistics run on the datasets to investigate the control of framework geology on the island geomorphology. The research continues to build on recent studies that have explored the use of EMI for mapping geology in coastal systems and control of framework geology on barrier island geomorphology at Padre Island. This is important research that contributes to the growing body of science on the influence that framework geology exerts on multiple time and space scales of barrier island response and evolution.

The research uses fairly complex statistics not commonly applied in coastal analyses, and the paper would benefit from including examples from other studies in the earth sciences that have used ARIMA approaches for similar applications. Rather than providing a 5-page statistics lesson (that would be more suited for a dissertation), I recommend reducing as much detail as possible and instead provide some real-world examples. This would also help provide justification for adopting these statistics. Why is this approach the best to test the hypothesis?

- We agree with the Reviewer that a discussion providing examples of how ARIMA models have been used in the earth sciences is missing from the paper. We removed some of the text and Equation 1 regarding the R/S analysis, as this is described in many places and is not the central statistical approach in the current study. Although we see the Reviewer's point that the statistical methods section is long, for completeness, we choose to leave the detailed explanation of the ARIMA statistics and equations in the paper, so the reader can see the mathematics described here without having to search the literature. However, we removed most of the discussion towards the end of this section to reduce the overall length. We also explain later in the Discussion section (via track-changes) that the reason why we chose to use ARIMA is because it is designed to handle both short and long-range correlations that other statistical models do not account for. Prior to the analysis, we did not know whether the series would contain any short-range correlations, thus, this is why we propose that the approach we chose is best to test the hypothesis. We added the following paragraph, which gives specific examples of how ARIMA has been successfully used in the earth sciences (new lines 420-433 in the revised paper).

*“ARIMA models are used across a wide range of disciplines in geoscience and have broad applicability for understanding the statistical structure of a given data series as it is related to some physical phenomenon (see Beran, 1992, 1994; Box and Jenkins, 1970; Cimino et al., 1999; Granger and Joyeux, 1980; Hosking, 1981; Taqqu et al., 1995). For example, Cimino et al. (1999) apply R/S analysis, ARIMA, and Neural Network analysis to different geological data sets including; tree ring data, Sr isotope data of Phanerozoic seawater samples, and El Niño phenomenon. The authors show that their statistical approach enables 1) recognition of qualitative changes within a given dataset, 2) evaluation of the scale (in)dependency of increments, 3) characterization of random processes that describe the evolution of the data, and 4) recognition of cycles embedded within the data series. In the soil sciences, Alemi et al. (1988) use ARIMA and Kriging to model the spatial variation of clay-cover thickness of a 78 km<sup>2</sup> area in northeast Iran and demonstrate that ARIMA modeling can adequately describe the nature of the spatial variations. ARIMA models have also been used to model periodicity of major extinction events in the geologic past (Kitchell and Pena, 1984).” ...*

Additionally, we added a discussion (new lines 818-826 in the paper) following the Reviewer's comment that the paper would benefit from a discussion of other methods to resolve geologic controls and why FARIMA was best, was chosen.

*... “To our knowledge, few framework geology studies have specifically used statistical testing to analyze correlations between subsurface geologic features and surface morphology. Two notable exceptions include Browder and McNinch (2006), and Schupp et al. (2006), both of which used chi-squared testing and cross-correlation analysis to quantify the spatial relationships between offshore bars, gravel beds, and/or paleo-channels at the Outer Banks, NC. Although these techniques are useful for determining spatial correlations between different data sets, they do not provide information about the scale (in)dependencies between the framework geology and surface geomorphology that FARIMA models are better designed to handle.”*

Although the authors provide a research objectives section, the paper is appears to be more exploratory than hypothesis-testing, presents previously established knowledge as new, and

there are statements in the early sections that are conclusion statements, giving the appearance of pre-conceived conclusions that drive the interpretation of statistics. For example, Pg 3, lines 69-72; Pg 10, lines 279-281; others as noted in comments in track changes. In addition, the work uses the same EMI data and beach metrics previously used by Wernette et al., 2018, but also includes higher resolution EMI and GPR data. Previous work by Weymer et al, 2016 and Wernette et al (2018) made the argument that EMI can be used to identify framework geology, so the present manuscript doesn't need to make that case and it should not be presented as a new conclusion, rather it can be stated that the findings corroborate the previous work.

- This was a careless mistake and we have made all of the suggested changes by the Reviewer in the paper to reflect that the results in the current study support previous research by this same author group. We also made the changes suggested by the Reviewer regarding the organization of the paper where there were conclusion statements in the Introduction, methods in the Discussion section, etc. Please refer to our specific responses to each comment in the track-changes version of the revised paper.

The manuscript is a bit long and because the details of the EMI data & collection, and the development of morphologic metrics have already been published (Weymer et al 2015; 2016; Wernette et al, 2018). Much of the detail in those sections can be condensed. This is indicated in the comments on pages 11-14. Condensing the statistics section (suggested above) will also help reduce the length of the paper.

- We agree with the Reviewer that much of this information can be found in our earlier work. We reduced as much detail as possible from the Methods sections and cited the appropriate studies that explain the methods in more detail (i.e., Weymer et al 2015; 2016; Wernette et al, 2018).

In the Discussion, it gets confusing at times what the paper is about. Is it about the EMI dataset and using it to map framework geology? Is it about the interpretation of the statistical data? Or is it using the combination of the latter to argue how framework geology controls island geomorphology?

- It is a combination of the latter to argue how the framework geology controls island geomorphology. Please refer to the changes we made in the Discussion, which should clarify these points made by the Reviewer.

There are several statements in the Discussion that this is the first time that EMI data can be interpreted to map framework geology, which has already been established in several recent papers (Weymer et al 2015; 2016; Wernette et al, 2018). The results of the FARIMA analysis are then used to support the findings that framework geology and island geomorphology both exhibit LRD at a regional scale, but less so on smaller scales. How is this finding useful and what might it tell us about the processes shaping barrier evolution. Smaller scales are similarly discussed and it is found that local scale (<10 km) geomorphology is influenced by geologic framework. Does this corroborate with findings at other barrier settings?

- Following similar comments mentioned above, we removed the statements in the Discussion saying that this is the first time the EMI data can be used to map the framework geology. Although each data series at the regional scale shows similar *d*-

values, the degree of LRD for the EMI spatial series is stronger at local scales within the paleo-channel region (refer to Table 3), suggesting that the framework geology controls are more significant at smaller (local) spatial scales < 10 km. These results suggest that the variable framework geology provides a structural control on beach-dune morphology similar to what has been observed on islands with a semi-regular framework geology (e.g. Santa Rosa Island, South Padre Island and Fire Island) (see Wernette et al., 2018).

The above are some of the major comments on the paper. I have provided an abundance of comments and suggestions in track changes on the e-manuscript. Note that I converted it to a Word document for the purposes of commenting and the formatting is impacted in some parts of the manuscript.

Please also note the supplement to this comment: <https://www.earth-surf-dynam-discuss.net/esurf-2018-5/esurf-2018-5-RC1-supplement.pdf>

- Thank you for your detailed comments and suggestions annotated throughout the text. Instead of listing each individual comment/suggestion in the rebuttal, we instead copied the comments from the supplementary pdf and added them to the revised manuscript with track changes. We provide a response to each comment immediately following the copied comment from the Reviewer. Please refer to the track-changes version of the revised manuscript for our responses.

**Figure 1:** The photo for the southern zone seems more representative of a storm impacted beach and not an example of the typical beach morphology.

- The southern zone of PAIS has numerous washover channels, especially within the last ~ 10 km and is largely erosive. We agree with the reviewer’s suggestion and modified the figure to show a more representative image of the beach-dune morphology typical of the southern zone of the island. Additionally, we included the approximate locations of where each photo was taken as indicated by the red dots.

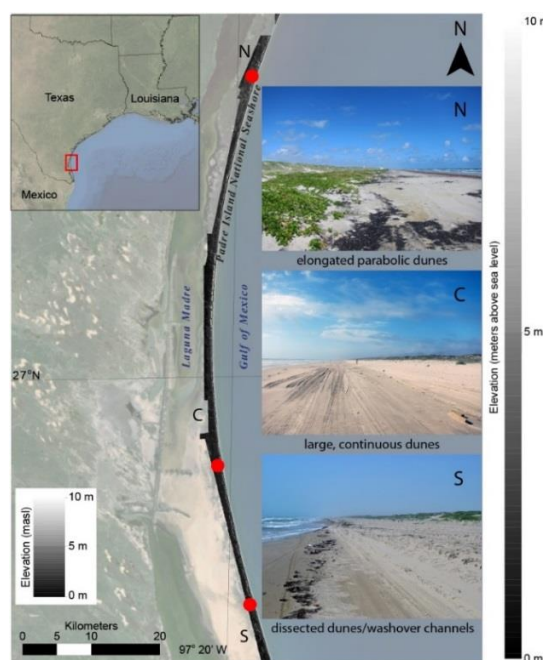


**Figure 2:** Please show where the photo & plot in b. are located in a.

- We highlighted the location of Plot B (white-dotted box) in Figure 2a as shown below in the modified figure.

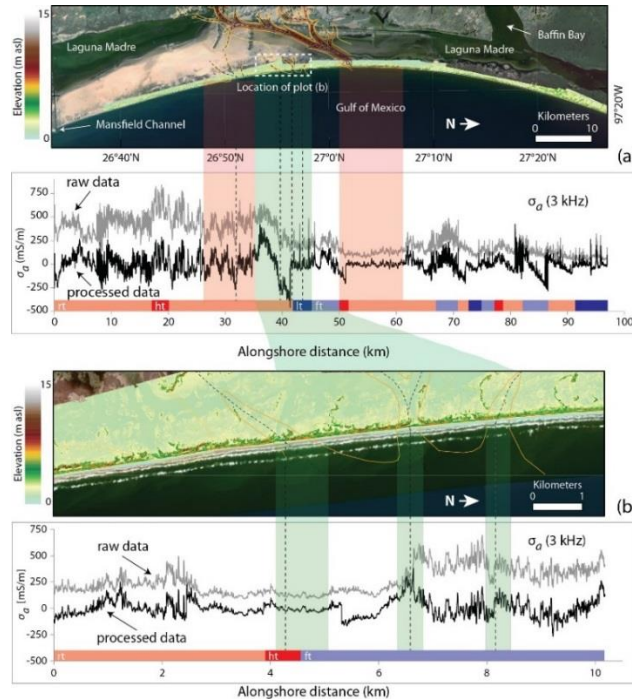


**Figure 3:** Highlight the interpretation of the bottom channel in the GPR data.

- We highlighted the interpretation of the bottom channel in yellow (see below).

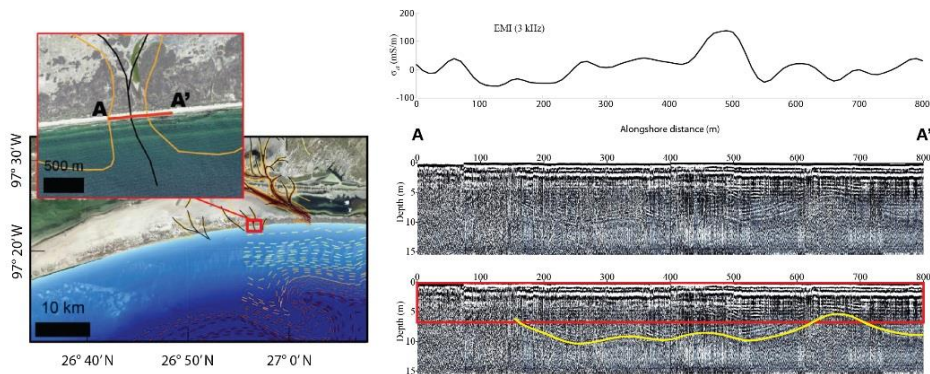
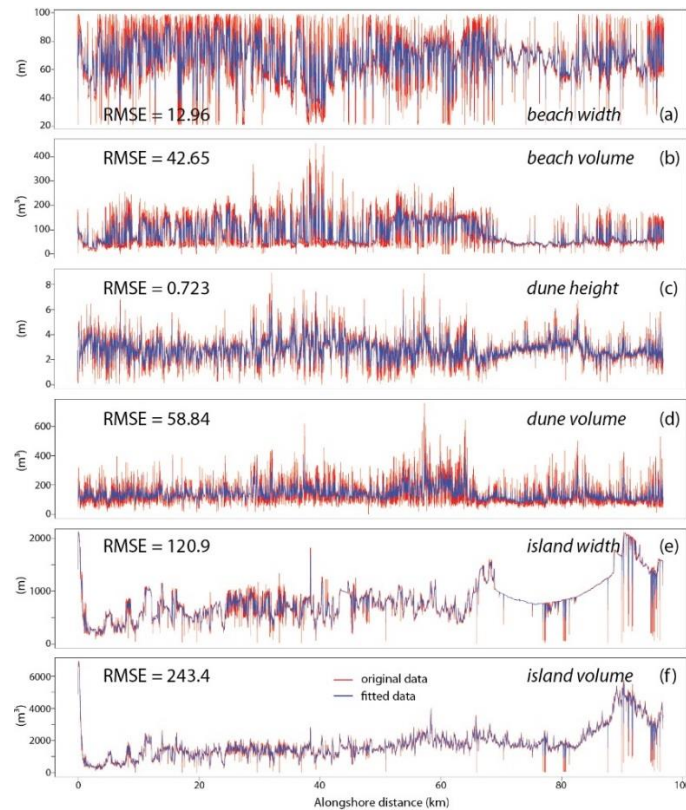


**Figure 7:** Would be helpful to add what each plot is on the plots themselves (e.g. beach width (bw); beach volume (bv) and so on).

- We added the description of each dataset directly on the plots (see modified figure below).



**REVIEWER #2:**

The paper presents a novel tool that utilizes electromagnetic methods to determine the alongshore variability of framework geology in barrier islands. The authors apply this novel approach (EMI geophysical profiling) to Padre Island (Texas), which is mostly in its natural state (except Malaquite beach). The results confirm some previous work by some of the co-authors, which suggests that barrier island change is scale could depend of the underlying geology. In particular the presence of paleo-channels. The authors support this result with a statistical analysis that demonstrates scale dependency at the intermediate scales (~ 30km), which matches the spacing between paleo-channels.

While the results are not surprising (as they confirm previous work by the authors), this manuscript is novel in its ability to integration electromagnetic, statistical, mapping and geomorphological methods. The paper is well written. In my opinion the manuscript is well suited for publication in Earth Surf.

**Response to Reviewer #2:**

- We thank the Reviewer for their constructive comments. Please refer to our responses to Reviewer #1 that echo similar remarks about our previous work in the study area.

1 **Statistical modeling of the long-range dependent structure of barrier island framework**  
2 **geology and surface geomorphology**

3 Bradley A. Weymer<sup>1,\*</sup>, Phillipe Wernette<sup>2</sup>, Mark E. Everett<sup>1</sup>, Chris Houser<sup>3</sup>

4 <sup>1</sup>Texas A&M University, Department of Geology and Geophysics, College Station, Texas  
5 77843, USA.

6 <sup>2</sup>Texas A&M University, Department of Geography, College Station, Texas 77843, USA.

7 <sup>3</sup>University of Windsor, Department of Earth and Environmental Sciences, Windsor, Ontario  
8 N9B 3P4, Canada.

9 *Correspondence to:* Bradley A. Weymer (brad.weymer@gmail.com) \*now at GEOMAR -  
10 Helmholtz Center for Ocean Research Kiel, Wischhofstraße 1-3, D-24148 Kiel, Germany

11  
12  
13  
14  
15  
16  
17  
18  
19  
20  
21  
22  
23  
24  
25  
26  
27  
28  
29  
30  
31  
32



33 **Abstract**

34 Shorelines exhibit long-range dependence (LRD) and have been shown in some environments to  
35 be described in the wavenumber domain by a power law characteristic of scale-independence.  
36 Recent evidence suggests that the geomorphology of barrier islands can, however, exhibit scale-  
37 dependence as a result of systematic variations of the underlying framework geology. The LRD of  
38 framework geology, which influences island geomorphology and its response to storms and sea  
39 level rise, has not been previously examined. Electromagnetic induction (EMI) surveys conducted  
40 along Padre Island National Seashore (PAIS), Texas, USA, reveal that the EMI apparent  
41 conductivity ( $\sigma_a$ ) signal and, by inference, the framework geology exhibits LRD at scales up to  $10^1$   
42 to  $10^2$  km. Our study demonstrates the utility of describing EMI  $\sigma_a$  and LiDAR spatial series by a  
43 fractional auto-regressive integrated moving average (ARIMA) process that specifically models  
44 LRD. This method offers a robust and compact way for quantifying the geological variations along  
45 a barrier island shoreline using three statistical parameters  $(p,d,q)$ . We discuss how ARIMA  
46  $(0,d,0)$ -models that use a single parameter  $d$  provide a quantitative measure for determining free  
47 and forced barrier island evolutionary behavior across different scales. Statistical analyses at  
48 regional, intermediate, and local scales suggest that the geologic framework within an area of  
49 paleo-channels exhibits a first-order control on dune height. The exchange of sediment amongst  
50 nearshore, beach and dune in areas outside this region are scale-independent, implying that barrier  
51 islands like PAIS exhibit a combination of free and forced behaviors that affect the response of the  
52 island to sea level rise.

53  
54  
55  
56  
57  
58  
59  
60  
61  
62

**Commented [WB1]:** Commented [A1]: Appropriate detail for abstract? Readers may be unfamiliar with the statistical approach since it is not common in the coastal community.  
**Response:** Added 'statistical' and deleted '(0,d,0)' for a more general ARIMA case



63

## 64 1 Introduction

65 Barrier island transgression in response to storms and sea-level rise depends to varying degrees on  
 66 pre-existing geologic features. The traditional assumption of uniform sand at depth and alongshore  
 67 cannot explain many of observations (e.g., Belknap and Kraft, 1985; Houser, 2012; Lentz and  
 68 Hapke, 2011; McNinch, 2004; Riggs et al., 1995). Models of barrier island evolution are required to  
 69 ascertain the degree to which the island is either *free* (such as a large sand body) or *forced* (i.e.  
 70 constrained) by the underlying geology. ~~Despite growing evidence that the underlying geological~~  
 71 ~~structure, otherwise termed *framework geology*, of barrier islands influences nearshore, beach and~~  
 72 ~~dune morphology (e.g., Belknap and Kraft, 1985; Houser, 2012; Lentz and Hapke, 2011; McNinch,~~  
 73 ~~2004; Riggs et al., 1995), this variable remains largely absent from shoreline change models that~~  
 74 ~~treat the geology as being uniform alongshore (e.g., Dai et al., 2015; Plant and Stockdon, 2012;~~  
 75 ~~Wilson et al., 2015). In a free system, small scale undulations in the dune line reinforce natural~~  
 76 ~~random processes that occur within the beach-dune system and are not influenced by the underlying~~  
 77 ~~geologic structure. In a forced system, the underlying geologic structure establishes boundary~~  
 78 ~~constraints that control how the island evolves over time.~~ Spatial variation in the height and position  
 79 of the dune line impacts the overall transgression of the island with sea-level rise (Sallenger, 2000).  
 80 Transgression is accomplished largely through the transport and deposition of beach and dune  
 81 sediments to the backbarrier as washover deposits during storms (Houser, 2012; Morton and  
 82 Sallenger Jr., 2003; Stone et al., 2004).

83

### 84 1.1 Framework geology controls on barrier island evolution

85 The dynamic geomorphology of a barrier island system is the result of a lengthy, complex and  
 86 ongoing history that is characterized by sea level changes and episodes of deposition and erosion  
 87 (e.g., Anderson et al., 2015; Belknap and Kraft, 1985; Rodriguez et al., 2001). Previous studies  
 88 demonstrate that the ~~underlying geological structure, otherwise termed *framework geology*~~  
 89 ~~*framework geology*~~ of barrier islands plays a considerable role in the evolution of these coastal  
 90 landscapes (Belknap and Kraft, 1985; Evans et al., 1985; Kraft et al., 1982; Riggs et al., 1995). For  
 91 example, antecedent structures such as paleo-channels, ravinement surfaces, offshore ridge and swale  
 92 bathymetry, and relict transgressive features (e.g., overwash deposits) have been suggested to

**Commented [WB2]: Commented [A2]:** Why? Are there refs for this or examples?

**Response:** Added more description of why the framework geology should be included and added appropriate refs

**Formatted:** Font: Not Italic

**Commented [WB3]: Commented [A3]:** Are there references for this? It appears that these statements are actually conclusions and don't belong here.

**Response:** Moved this sentence to the conclusions section

**Commented [WB4]: Commented [A4]:** Height or position or both?

**Response:** both

**Formatted:** Font: Not Bold

93 influence barrier island geomorphology over a wide range of spatial scales (Hapke et al., 2010;  
94 Hapke et al., 2016; Houser, 2012; Lentz and Hapke, 2011; McNinch, 2004). In this study, the term  
95 “framework geology” is specifically defined as the topographic surface of incised valleys, paleo-  
96 channels, and/or the depth to ravinement surface beneath the modern beach.

97 As noted by Hapke et al. (2013), the framework geology at the **regional scale** (> 30 km)  
98 influences the geomorphology of an entire island. Of particular importance are the location and size  
99 of glacial, fluvial, tidal, and/or inlet paleo-valleys and channels (Belknap and Kraft, 1985; Colman et  
100 al., 1990; Demarest and Leatherman, 1985), and paleo-deltaic systems offshore or beneath the  
101 modern barrier system (Coleman and Gagliano, 1964; Frazier, 1967; Miselis et al., 2014; Otvos and  
102 Giardino, 2004; Twichell et al., 2013). At the regional scale, nonlinear hydrodynamic interactions  
103 between incident wave energy and nearshore ridge and swale bathymetric features can generate  
104 periodic alongshore variations in beach-dune morphology (e.g., Houser, 2012; McNinch, 2004)  
105 that are superimposed on larger-scale topographic variations as a result of transport gradients  
106 (Tebbens, et al., 2002). At the **intermediate scale** (10 - 30 km), feedbacks between geologic  
107 features and relict sediments of the former littoral system (e.g., Honeycutt and Krantz, 2003;  
108 Riggs et al., 1995; Rodriguez et al., 2001; Schwab et al., 2000) act as an important control on  
109 dune formation (Houser et al., 2008) and offshore bathymetric features (e.g., Browder &  
110 McNinch, 2006; Schwab et al., 2013). Framework geology at the **local scale** ( $\leq 10$  km), induces  
111 meso ( $\sim 10^1 - 10^2$  m) to micro-scale ( $< 1$  m) sedimentological changes (e.g., Murray and Thieler,  
112 2004; Schupp, et al., 2006), variations in the thickness of shoreface sediments (Brown and  
113 Macon, 1977; Miselis and McNinch, 2006), and spatial variations in sediment transport across  
114 the island (Houser and Mathew, 2011; Houser, 2012; Lentz and Hapke, 2011).

115 To date, most of what is known regarding barrier island framework geology is based on  
116 studies done at either intermediate or local scales (e.g., Hapke et al., 2010; Lentz and Hapke, 2011;  
117 McNinch, 2004) whereas few studies exist at the regional scale for United States coastlines (Hapke et  
118 al., 2013). The current study focuses on barrier islands in the US and we do not consider work on  
119 barrier islands in other regions. Assessments of framework geology at regional and intermediate  
120 spatial scales for natural and anthropogenically-modified barrier islands are essential for improved  
121 coastal management strategies and risk evaluation since these require a good understanding of the  
122 connections between subsurface geology and surface morphology. For example, studies by Lentz and

123 Hapke (2011); Lentz et al., (2013) at Fire Island, New York suggest that the short-term  
124 effectiveness of engineered structures is likely influenced by the framework geology. Extending  
125 their work, Hapke et al. (2016) identified distinct patterns of shoreline change that represent  
126 different responses alongshore to oceanographic and geologic forcing. These authors applied  
127 empirical orthogonal function (EOF) analysis to a time series of shoreline positions to better  
128 understand the complex multi-scale relationships between framework geology and contemporary  
129 morphodynamics. Gutierrez et al. (2015) used a Bayesian network to predict barrier island  
130 geomorphic characteristics and argue that statistical models are useful for refining predictions of  
131 locations where particular hazards may exist. These examples demonstrate the benefit of using  
132 statistical models as quantitative tools for interpreting coastal processes at multiple spatial and  
133 temporal scales (Hapke et al., 2016).

134

#### 135 1.2 Statistical measures of coastline geomorphology

136 It has long been known that many aspects of landscapes exhibit similar statistical properties  
137 regardless of the length or time scale over which observations are sampled (Burrough, 1981). An  
138 often-cited example is the length  $L$  of a rugged coastline (Mandelbrot, 1967), which increases  
139 without bound as the length  $G$  of the ruler used to measure it decreases, in rough accord with the  
140 formula  $L(G) \sim G^{1-D}$ , where  $D \geq 1$  is termed the fractal dimension of the coastline. Andrieu  
141 (1996), however, has identified limitations of the self-similar coastline concept, suggesting that a  
142 coastline may contain irregularities that are concentrated at certain characteristic length-scales  
143 owing to local processes or structural controls. Recent evidence from South Padre Island, Texas  
144 (Houser and Mathew, 2011), Fire Island, New York (Hapke et al., 2010), and Santa Rosa Island,  
145 Florida (Houser et al., 2008) suggests that the geomorphology of barrier islands is affected to  
146 varying degrees by the underlying framework geology and that this geology varies, often with  
147 periodicities, over multiple length-scales. The self-similarity of the framework geology and its  
148 impact on the geomorphology of these barrier islands was not examined explicitly.

149 Many lines of evidence suggest that geological formations in general are inherently rough  
150 (i.e., heterogeneous) and contain multi-scale structure (Bailey and Smith, 2005; Everett and  
151 Weiss, 2002; Radliński et al., 1999; Schlager, 2004). Some of the underlying geological factors  
152 that lead to self-similar terrain variations are reviewed by Xu et al. (1993). In essence, competing

153 and complex morphodynamic processes, influenced by the underlying geological structure,  
154 operate over different spatiotemporal scales, such that the actual terrain is the result of a complex  
155 superposition of the various effects of these processes (see Lazarus et al., 2011). Although no  
156 landscape is strictly self-similar on all scales, Xu et al. (1993) show that the fractal dimension, as  
157 a global morphometric measure, captures multi-scale aspects of surface roughness that are not  
158 evident in conventional local morphometric measures such as slope gradient and profile  
159 curvature.

160 With respect to coastal landscapes, it has been suggested that barrier shorelines are scale  
161 independent, such that the wavenumber spectrum of shoreline variation can be approximated by  
162 a power law at alongshore scales from tens of meters to several kilometers (Lazarus et al., 2011;  
163 Tebbens et al., 2002). However, recent findings by Houser et al. (2015) suggest that the beach-  
164 dune morphology of barrier islands in Florida and Texas is scale-dependent and that  
165 morphodynamic processes operating at swash (0-50 m) and surf-zone (< 1000 m) scales are  
166 different than the processes operating at larger scales. In this context, scale-dependence implies  
167 that a certain number of different processes are simultaneously operative, each process acting at  
168 its own scale of influence, and it is the superposition of the effects of these multiple processes  
169 that shapes the overall behavior and shoreline morphology. This means that shorelines may have  
170 different patterns of irregularity alongshore with respect to barrier island geomorphology, which  
171 has important implications for analyzing long-term shoreline retreat and island transgression.  
172 Lazarus et al. (2011) point out that deviations from power law scaling at larger spatial scales  
173 (tens of km) emphasizes the need for more studies that investigate large-scale shoreline change.  
174 While coastal terrains might not satisfy the strict definition of self-similarity, it is reasonable to  
175 expect them to exhibit long-range dependence (LRD). LRD pertains to signals in which the  
176 correlation between observations decays like a power law with separation, i.e. much slower than  
177 one would expect from independent observations or those that can be explained by a short-  
178 memory process, such as an autoregressive-moving-average (ARMA) with small  $(p,q)$  (Beran,  
179 1994; Doukhan et al., 2003).

180

181 1.3 Research objectives

182 This study performed at Padre Island National Seashore (PAIS), Texas, USA utilizes  
183 electromagnetic induction (EMI) apparent conductivity  $\sigma_a$  responses to provide insight into the  
184 relation between spatial variations in framework geology and surface morphology. Two  
185 alongshore EMI surveys at different spatial scales (100 km and 10 km) were conducted to test  
186 the hypothesis that, like barrier island morphology, subsurface framework geology exhibits LRD  
187 characteristic of scale-independence. The  $\sigma_a$  responses, which are sensitive to parameters such as  
188 porosity and mineral content, are regarded herein as a rough proxy for subsurface framework  
189 geology (Weymer et al., 2015a). This assumes, of course, that alongshore variations in salinity  
190 and water saturation, and other factors that shape the  $\sigma_a$  response, can be neglected to first order.  
191 A corroborating 800 m ground-penetrating radar (GPR) survey, providing an important check on  
192 the variability observed within the EMI signal, confirms the location of a previously identified  
193 paleo-channel (Fisk, 1959) at  $\sim 5 - 10$  m depth. The overall geophysical survey design allows for  
194 a detailed evaluation of the long-range-dependent structure of the framework geology over a  
195 range of length scales spanning several orders of magnitude. We explore the applicability of  
196 autoregressive integrated moving-average (ARIMA) processes as ~~statistical~~ models that describe  
197 the statistical connections between EMI and Light Detection and Ranging (LiDAR) spatial data  
198 series. This paper ~~utilizes~~ introduces the use of a generalized fractional ARIMA (0,d,0) process  
199 (Hosking, 1981) that is specifically designed to model LRD for a given data series using a single  
200 differencing non-integer parameter  $d$ . The parameter  $d$  can be used in the present context to  
201 discriminate between *forced*, scale-dependent controls by the framework geology; i.e., stronger  
202 LRD ( $d \rightarrow 0.5$ ) and *free* behavior that is scale-independent; i.e., weaker LRD ( $0 \leftarrow d$ ). In other  
203 words, it is the particular statistical characteristics of the framework geology LRD at PAIS that  
204 we are trying to ascertain from the EMI  $\sigma_a$  signal, with the suggestion that  $\sigma_a$  measurements can  
205 be used similarly at other sites to reveal the hidden LRD characteristics of the framework  
206 geology.

207

## 208 2 Background and regional setting

### 209 2.1 Utility of electromagnetic methods in coastal environments

210 Methods to ascertain the alongshore variability of framework geology, and to test long-range  
211 dependence, are difficult to implement and can be costly. Cores provide detailed point-wise

Commented [WB5]: Commented [A5]: Why, specifically, is it important to know this?

Response: We are testing this at different spatial scales to see whether the framework geology is scale-dependent, or scale-independent at all scales or at specific scales. To clarify, we added 'characteristic of scale-independence.'

Commented [WB6]: Commented [A6]: Tell the reader why you are doing this.

Response: fixed

212 geologic data; however, they do not provide laterally continuous subsurface information (Jol et  
213 al., 1996). Alternatively, geophysical techniques including seismic and GPR provide spatially  
214 continuous stratigraphic information (e.g., Buynevich et al., 2004; Neal, 2004; Nummedal and  
215 Swift, 1987; Tamura, 2012), but they are not ideally suited for LRD testing because the data  
216 combine depth and lateral information at a single acquisition point. Moreover, GPR signals  
217 attenuate rapidly in saltwater environments whereas seismic methods are labor-intensive and  
218 cumbersome. On the other hand, terrain conductivity profiling is an easy-to-use alternative that  
219 has been used in coastal environments to investigate fundamental questions involving;  
220 instrument performance characteristics (Delefortrie et al., 2014; Weymer et al., 2016),  
221 groundwater dynamics (Stewart, 1982; Fitterman and Stewart, 1986; Nobes, 1996; Swarzenski,  
222 and Izbicki, 2009), and framework geology (Seijmonsbergen et al. 2004; Weymer et al. 2015).  
223 Previous studies combining EMI with either GPR (Evans and Lizarralde, 2011) or coring  
224 (Seijmonsbergen et al. 2004) demonstrate the validity of EM measurements as a means to  
225 quantify alongshore variations in the framework geology of coastlines.

226 In the alongshore direction, Seijmonsbergen et al. (2004) used a Geonics EM34™ terrain  
227 conductivity meter ~~oriented in the horizontal dipole mode with intercoil separation and station~~  
228 ~~spacing both of 20 m. This configuration provides an exploration depth of roughly 15 m. A 14.5~~  
229 ~~km length EMI transect was collected along the backbeach~~ crossing a former outlet of the Rhine  
230 River, Netherlands to evaluate alongshore variations in subsurface lithology. The survey was  
231 conducted in an area that was previously characterized by drilling and these data were used to  
232 calibrate the  $\sigma_a$  measurements. The results from the study suggest that coastal sediments can be  
233 classified according to  $\sigma_a$  signature ~~and. The range of  $\sigma_a$  values was categorized into three groups.~~  
234 ~~The first group of low  $\sigma_a$  20–45 millisiemens per meter (mS/m) with low variability amplitudes was~~  
235 ~~interpreted as beach sands. The second group of medium  $\sigma_a$  values (20–90 mS/m) with large~~  
236 ~~variability corresponded to clay and peat layers of varying thickness. A third group of high  $\sigma_a$  values~~  
237 ~~(60–190 mS/m) with large variability was interpreted as clay-rich brackish channel deposits. The~~  
238 ~~authors suggest~~ that high  $\sigma_a$  values occur in areas where the underlying conductive layer is thick and  
239 close to the surface. Although Seijmonsbergen et al. (2004) ~~propose~~ ~~suggest~~ that EMI surveys are a  
240 rapid, inexpensive method to investigate subsurface lithology they also acknowledge that variations  
241 in salinity as a result of changing hydrologic conditions, storm activity and/or tidal influence

242 confound the geological interpretation and should be investigated in further detail (see Weymer et al.,  
243 2016).

244 The challenge on many barrier islands and protected National Seashores is obtaining  
245 permission for extracting drill cores to validate geophysical surveys. At PAIS, numerous areas  
246 along the island are protected nesting sites for the endangered Kemp's ridley sea turtle,  
247 migratory birds, while other areas comprise historic archeological sites with restricted access.  
248 Thus, coring is not allowed and only non-invasive techniques, such as EMI/GPR are permitted.

249

## 250 2.2 Regional setting

251 North Padre Island is part of a large arcuate barrier island system located along the Texas Gulf of  
252 Mexico coastline ~~and is the longest undeveloped barrier island in the world~~. The island is one of  
253 ten national seashores in the United States and is protected and managed by the National Park  
254 Service, a bureau of the Department of the Interior. PAIS is 129 km in length, and is an ideal  
255 setting for performing EMI surveys because there is minimal cultural noise to interfere with the  
256  $\sigma_a$  signal, which as stated earlier we regard as a proxy for alongshore variations in framework  
257 geology (Fig. 1). Additionally, ~~there is high-resolution elevation data available from a 2009~~  
258 ~~aerial LiDAR survey, island is well covered by high-resolution aerial LiDAR data~~. The island is  
259 not dissected by inlets or navigation channels (excluding Mansfield Channel separating north and  
260 south Padre Island), or modified by engineered structures (e.g., groynes, jetties, etc.) that often  
261 interfere with natural morphodynamic processes (see Talley et al., 2003). The above  
262 characteristics make the study area an exceptional location for investigating the relationships  
263 between large-scale framework geology and surface morphology.

264 ~~Relatively little is known about the framework geology at PAIS, especially its alongshore~~  
265 ~~variability. A notable exception is the information obtained from a series of coring and seismic~~  
266 ~~surveys conducted by Fisk (1959) in the central region of Padre Island (~27° N).~~ As described in  
267 Weymer et al. (2015a; Fig. 3), locations of several paleo-channels were established by Fisk  
268 (1959) based on 3,000 cores and ~~several~~ seismic surveys. More than 100 borings were drilled to  
269 the top of the late Pleistocene surface (tens of m depth) providing sedimentological data for  
270 interpreting the depth and extent of the various paleo-channels. These cores were extracted ~ 60

**Commented [WB7]:** Commented [A7]: The level of detail can be significantly reduced.

**Response:** fixed

**Commented [WB8]:** Commented [A8]: The EMI data, the recent pubs by Weymer and Wernette, and the original studies by Fisk contradict this statement.

**Response:** deleted these statements

**Commented [WB9]:** Commented [A9]: Figure 2?

**Response:** No, Figure 3 is correct



271 years ago, but the remnant Pleistocene and Holocene fluvial/deltaic features described in Fisk's  
272 study likely have not changed over decadal time scales.

273 Geologic interpretations based on the Fisk (1959) data suggest that the thickness of the  
274 modern beach sands is ~ 2 – 3 m, and they are underlain by Holocene shoreface sands and muds  
275 to a depth of ~ 10 – 15 m (Brown and Macon, 1977; Fisk, 1959). The Holocene deposits lie upon  
276 a Pleistocene ravinement surface of fluvial-deltaic sands and muds and relict transgressive  
277 features. A network of buried valleys and paleo-channels in the central segment of the island, as  
278 interpreted by Fisk (1959), exhibits a dendritic, tributary pattern. The depths of the buried valleys  
279 inferred from seismic surveys range from ~ 25 – 40 m (Brown and Macon, 1977). These  
280 channels have been suggested to incise into the Pleistocene paleo-surface and became infilled  
281 with sands from relict Pleistocene dunes and fluvial sediments reworked by alongshore currents  
282 during the Holocene transgression (Weise and White, 1980). However, the location and cross-  
283 sectional area of each valley and paleo-channel alongshore is not well-constrained. It is also  
284 possible that other channels exist other than those identified by Fisk (1959).

285 As ~~suggested~~presented in Weymer et al. (2015a), minima in the alongshore  $\sigma_a$  signal are  
286 spatially correlated with the locations of these previously identified geologic features. This  
287 observation provides an impetus for using EMI to map the known, and any previously  
288 unidentified, geologic features alongshore. ~~The observed beach dune morphology and other~~  
289 ~~metrics such as island width are highly variable and controlled to an unknown extent by the~~  
290 ~~framework geology both within and outside the known paleo-channel regions. The fact that~~  
291 ~~much of the framework geology at PAIS is poorly known provides additional motivation for~~  
292 ~~integrating subsurface geophysical methods and surface observations to analyze, from a~~  
293 ~~statistical standpoint, the key geologic controls on island morphology within the study area.~~

294

### 295 3 Methods

296 A combination of geophysical, geomorphological, and statistical methods are used in this study  
297 to quantify the relationships between framework geology and surface geomorphology at PAIS. A  
298 description of the EMI, GPR, geomorphometry and statistical techniques is provided in the  
299 following sections.

300

**Commented [WB10]:** Commented [A10]: This is one of the paper's conclusions and does not belong here. Otherwise, provide a reference for this statement.

**Response:** deleted

### 3.1 Field EMI and GPR surveys

Profiles of EMI  $\sigma_a$  responses typically are irregular and each datum represents a spatial averaging of the bulk subsurface electrical conductivity  $\sigma$ , which in turn is a function of a number of physical properties (e.g., porosity, lithology, water content, salinity, etc.). The “sensor footprint”, or subsurface volume over which the spatial averaging is performed, is dependent on the separation between the TX – RX coils (1.21 m in this study), and the transmitter frequency. The horizontal extent, or radius, of the footprint can be more or less than the step-size between subsequent measurements along the profile. The sensor footprint determines the volume of ground that contributes to  $\sigma_a$  at each acquisition point, and as will be discussed later, the radius of the footprint has important implications for analyzing LRD. The footprint radius depends on frequency and ground conductivity, but is likely to be of the same order as, but slightly larger than, the intercoil spacing. Two different station-spacings were used to examine the correlation structure of  $\sigma_a$  as a function of spatial scale. An island-scale alongshore survey of ~ 100 km length was performed using a 10 m station spacing (station spacing  $\gg$  footprint radius) such that each  $\sigma_a$  measurement was recorded over an independently sampled volume of ground. Additionally, a sequence of  $\sigma_a$  readings was collected at 1 m spacing (station spacing  $<$  footprint radius) over a profile length of 10 km within the Fisk (1959) paleo-channel region of the island. This survey design allows for comparison of the long-range-dependent structure of the framework geology over several orders of magnitude ( $10^0 - 10^5$  m).

The 100-km-long alongshore EMI survey was performed during a series of three field campaigns, resulting in a total of 21 (each of length ~ 4.5 km) segments that were collected during October 9 – 12<sup>th</sup>, 2014, November 15 – 16<sup>th</sup>, 2014, and March 28<sup>th</sup>, 2015. The EMI  $\sigma_a$  profiles were stitched together by importing GPS coordinates from each measurement into ArcGIS™ to create a single composite spatial data series. The positional accuracy recorded by a TDS Recon PDA equipped with a Holux™ WAAS GPS module was found to be accurate within ~ 1.5 m. To reduce the effect of instrument drift caused by temperature, battery and other systematic variations through the acquisition interval, a drift correction was applied to each segment, the segments were then stitched together, following which a regional linear trend removal was applied to the composite dataset. An additional 10 km survey was performed along a segment of the same 100 km survey line in one day on March 29<sup>th</sup>, 2015, to determine whether

**Commented [WB11]:** Commented [A11]: This section should be scaled down. The details about the EMI data and collection have been presented in earlier papers by same authors/co-authors.

**Response:** fixed

331 ~~varying hydrologic conditions in both space and time, which are discussed below, play a~~  
332 ~~deleterious role in resolving the framework geology.~~ This second composite data series consists  
333 of 8 stitched segments.

**Commented [WB12]:** Commented [A12]: Wasn't this the basis of Weymer, 2016?

**Response:** Yes. Deleted the last part of this sentence

334 The same multi-frequency GSSI Profiler EMP-400™ instrument was used for each  
335 segment. All transects were located in the backbeach environment ~ 25 m inland from the mean  
336 tide level (MTL). ~~This location was chosen to reduce the effect of changing groundwater~~  
337 ~~conditions in response to nonlinear tidal forcing (see Weymer et al., 2016), which may be~~  
338 ~~significant closer to the shoreline. The sensor has reduced ability to detect lateral changes in the~~  
339 ~~underlying geology during wet conditions such as during or immediately after significant rainfall~~  
340 ~~events, or at high tide near the shoreline, since electrical conductivity increases rapidly with~~  
341 ~~water content. The transect locations also avoid the large topographic variations (see Santos et~~  
342 ~~al., 2009) fronting the foredune ridge that can reduce the efficiency of data acquisition and~~  
343 ~~influence the EMI signal. In a companion study, Weymer et al. (2016) demonstrated that the  $\sigma_a$~~   
344 ~~signal at the beachfront exhibits a step-like response over the course of a tidal cycle; however,~~  
345 ~~this effect is less pronounced further inland where the surveys in the present study were~~  
346 ~~collected. Their study demonstrates that the difference between high tide and low tide EMI  $\sigma_a$~~   
347 ~~measurements is as large as 50 mS/m at the backbeach, but this difference is less than 9% of the~~  
348 ~~range of  $\sigma_a$  variations observed (— 50 — 600 mS/m) along the entire length of the island. As will~~  
349 be shown later, there is not a direct correlation between high tide and high  $\sigma_a$  values. Thus, we  
350 assume the tidal influence on the EMI signal can be neglected over the spatial scales of interest  
351 in the present study. Nevertheless, the duration and approximate tidal states of each survey was  
352 documented in order to compare with the EMI signal (see Weymer et al., 2016). Tidal data were  
353 accessed from NOAA's Tides and Currents database (NOAA, 2015b). Padre Island is microtidal  
354 and the mean tidal range within the study area is 0.38 m (NOAA, 2015a). A tidal signature in EMI  
355 signals may become more significant at other barrier islands with larger tidal ranges.

**Commented [WB13]:** Commented [A13]: Condense and cite Weymer et al, 2016

**Response:** Fixed

356 For all surveys, the EMI profiler was used in the same configuration and acquisition  
357 settings as described in Weymer et al. (2016). a vertical dipole orientation with TX and RX coils  
358 aligned in the (P mode) direction parallel to the profile line (Weymer et al., 2016). The transect  
359 locations were chosen to also avoid the large topographic variations (see Santos et al., 2009)  
360 fronting the foredune ridge that can reduce the efficiency of data acquisition and influence the

361 EMI signal. Measurements were made at a constant step-size to simplify the data analysis; for  
362 example, ARIMA models require that data are taken at equal intervals (see Cimino et al., 1999).  
363 ~~The EMI profiler was carried at a height of 0.7 m above the ground to mitigate noise from the~~  
364 ~~mainly non-metallic debris on the beach that unfortunately is scattered along the island (Weymer~~  
365 ~~et al., 2016). Although the sensor is capable of recording three frequencies simultaneously (see~~  
366 ~~Geophysical Survey Systems, 2007), we~~ choose herein to focus on data collected at 3 kHz,  
367 resulting in a depth of investigation (DOI) of ~ 3.5 – 6.4 m over the range of conductivities  
368 found within the study area (Weymer et al., 2016; Table 1.). Because the depth of the modern  
369 beach sands is ~ 2 – 3 m or greater (see Brown and Macon, 1977; page 56, Figure 15), variations  
370 in the depth to shoreface sands and muds is assumed to be within the DOI of the profiler, which  
371 may not be captured at the higher frequencies also recorded by the sensor (i.e., 10, and 15 kHz).

Commented [WB14]: Commented [A14]: Garbage or rack or ??

Response: both, but we decided to delete this sentence as this information is already described in Weymer et al. 2016

372 An 800 m GPR survey was performed on August 12<sup>th</sup>, 2015 across one of the paleo-  
373 channels previously identified Fisk (1959) located within the 10 km EMI survey for comparison  
374 with the  $\sigma_a$  measurements. We used a Sensors and Software PulseEKKO Pro<sup>®</sup> system for this  
375 purpose. A survey grade GPS with a positional accuracy of 10 cm was used to match the  
376 locations and measurements between the EMI/GPR surveys. Data were acquired in reflection  
377 mode at a nominal frequency of 100 MHz with a standard antenna separation of 1 m and a step-  
378 size of 0.5 m. The instrument settings resulted in a DOI of up to 15 m. Minimal processing was  
379 applied to the data and includes a dewow filter and migration (0.08 m/ns), followed by AGC gain  
380 (see Neal, 2004). ~~Given~~ The theory and operational principles of GPR are discussed in many  
381 places (e.g. Everett, 2013; Jol, 2008) and will not be reviewed here.

Commented [WB15]: Commented [A15]: Condense and cite Weymer et al, 2016

Response: fixed

### 382 383 3.2 Geomorphometry

384 Topographic information was extracted from aerial LiDAR data that were collected by the Army  
385 Corps of Engineers (USACE) in 2009 as part of the West Texas Aerial Survey project to assess  
386 post-hurricane conditions of the beaches and barrier islands along the Texas coastline. This  
387 dataset is the most recent publicly available LiDAR survey of PAIS and it provides essentially  
388 complete coverage of the island. With the exception of Hurricane Harvey, which made landfall  
389 near Rockport, Texas as a Category 4 storm in late August, 2017, Padre Island has not been  
390 impacted by a hurricane since July 2008, when Hurricane Dolly struck South Padre Island as a

391 Category 1 storm (NOAA, 2015a). The timing of the LiDAR and EMI surveys in this study  
392 precede the impacts of Hurricane Harvey, and it is assumed that the surface morphology across  
393 the island at the spatial scales of interest (i.e.,  $10^1 - 10^2$  km) did not change appreciably between  
394 2009 and 2015.

395 A 1-m resolution DEM was created from 2009 LiDAR point clouds available from  
396 NOAA's Digital Coast (NOAA, 2017). The raw point cloud tiles were merged to produce a  
397 combined point cloud of the island within the park boundaries of the PAIS National Seashore.  
398 The point clouds were processed into a continuous DEM using the ordinary kriging algorithm in  
399 SAGA GIS, which is freely available open-source software ([www.saga-gis.org/](http://www.saga-gis.org/)); and subsequent  
400 terrain analysis was conducted using an automated approach involving the relative relief (RR)  
401 metric (Wernette et al., 2016). Several morphometrics including beach width, dune height, and  
402 island width were extracted from the DEM by averaging the RR values across window sizes of  
403 21 m x 21 m, 23 m x 23 m, and 25 m x 25 m. The choice of window size is based on tacit a  
404 priori knowledge and observations of the geomorphology in the study area. A detailed  
405 description of the procedure for extracting each metric is provided in Wernette et al. (2016).

406 Relative relief is a measure of topographic position of the center pixel compared to the  
407 minimum and maximum pixel elevations within a given computational window. Several other  
408 morphometrics including beach width, dune height, and island width were extracted from the  
409 DEM using a recently developed automated multi-scale approach (see Wernette et al., 2016).  
410 This technique extracts the open water shoreline (in this case the Gulf of Mexico shoreline) and  
411 backbarrier shoreline based on elevation thresholds and uses them to calculate beach and island  
412 width referenced to mean sea level (MSL). Dune metrics including dune crest, dune heel, and  
413 dune toe elevations are calculated based on the average relative relief (RR) to determine where  
414 the dune begins, crests, and ends along every shore-normal profile in a DEM. This process is  
415 repeated for all such profiles at a 1 m spacing along the entire length of PAIS to generate a  
416 continuous dataset of alongshore dune height and volume. A detailed description of the  
417 procedure for extracting each metric is provided in Wernette et al. (2016).

418 Each morphometric feature was extracted by averaging the RR values across window  
419 sizes of 21 m x 21 m, 23 m x 23 m, and 25 m x 25 m. The choice of window size is based on  
420 tacit a priori knowledge and observations of the geomorphology in the study area. Larger

**Commented [WB16]: Commented [A16]:** What was the reason for not just downloading the 1-m DEM from NOAA? What was gained by creating a DEM from point cloud?

**Response:** The main reason why we created a 1m DEM is because it is much more accurate (vertically and horizontally) than the 10m products. Additionally, we wanted to be able to pick out finer changes in beach-dune-island morphology than a 10m DEM would allow. Essentially, we were able to generate a better DEM all around (spatial resolution, vertical accuracy, and horizontal accuracy).

421 window sizes will better capture smoother beach and dune features by reducing sensitivity to the  
422 fine-scale variability induced by measurement error inherent in LiDAR-derived DEMs, as well  
423 as natural terrain irregularities (Wernette et al., 2016). Each DEM series is paired with the  $\sigma_a$   
424 profile by matching the GPS coordinates (latitude and longitude) recorded in the field by the  
425 EMI sensor. Cross-sectional elevation/DEM profiles oriented perpendicular to the shoreline were  
426 analyzed every 10 m (y-coordinate) along the EMI profile to match the same 10 m sampling  
427 interval of the  $\sigma_a$  measurements. The terrain variations along each cross-shore profile are  
428 summed to calculate beach and island volume based on the elevation thresholds mentioned  
429 above. Dune volume is calculated by summing the pixel elevations starting at the dune toe,  
430 traversing the dune crest, and ending at the dune heel. In total, six DEM morphometrics were  
431 extracted as spatial data series to be paired with the EMI data, each having an identical sample  
432 size ( $n = 9,694$ ), which is sufficiently large for statistical ARIMA modeling.

433

### 434 3.3 Statistical methods

435 Although the procedures for generating the EMI and LiDAR datasets used in this study  
436 are different, the intended goal is the same; to produce spatial data series that contain similar  
437 numbers of observations for comparative analysis using a combination of signal processing and  
438 statistical modeling techniques. The resulting signals comprising each data series represent the  
439 spatial averaging of a geophysical (EMI) or geomorphological (~~DEM~~elevation) variable that  
440 contains information about the important processes-form relationships between subsurface  
441 geologic features and island geomorphology that can be teased out by means of comparative  
442 analysis (Weymer et al., 2015a). Because we are interested in evaluating these connections at  
443 both small and large spatial scales, our first approach is to determine the autocorrelation function  
444 and Hurst coefficient (self-similarity parameter)  $H$  and hence verify whether the data series are  
445 characterized by short and/or long-range memory (Beran, 1992; Taqqu et al., 1995). LRD occurs  
446 when the autocorrelation within a series, at large lags, tend to zero like a power function, and so  
447 slowly that the sums diverge (Doukhan et al., 2003). LRD is often observed in natural time series  
448 and is closely related to self-similarity, which is a special type of LRD.

449 The degree of LRD is related to the scaling exponent,  $H$  of a self-similar process, where  
450 increasing  $H$  in the range  $0.5 < H \leq 1.0$  indicates an increasing tendency towards such an effect

**Commented [WB17]: Commented [A17]:** The DEM is the grid.  
The profile is elevation extracted from the grid.

**Response:** fixed

**Commented [WB18]: Commented [A18]:** Condense and state  
that you are using the topographic dataset generated by Wernette

**Response:** fixed

**Commented [WB19]: Commented [A19]:** It would be very  
helpful for readers not familiar with the fairly complex statistical  
approach to provide examples of their application in earth science  
and perhaps not present a full lesson ARIMA on the stats.

**Response:** We agree and added some examples in the paragraph  
below (new lines 420-433). Please also refer to our response to this  
comment in the rebuttal letter.

**Formatted:** Default, Indent: First line: 0.5"

451 (Taqqu, 2003). Large correlations at small lags can easily be detected by models with short-  
 452 memory (e.g., ARMA, Markov processes) (Beran, 1994). Conversely, when correlations at large  
 453 lags slowly tend to zero like a power function, the data contain long-memory effects and either  
 454 fractional Gaussian noise (fGn), or ARIMA models may be suitable (Taqqu et al., 1995). The  
 455 R/S statistic is the quotient of the range of values in a data series and the standard deviation  
 456 (Beran, 1992, 1994; Hurst, 1951; Mandelbrot and Taqqu, 1979). When plotted on a log/log plot,  
 457 the resulting slope of the best-fit line gives an estimate of  $H$ , which is useful as a diagnostic tool  
 458 for estimating the degree of LRD (see Beran, 1994). The degree of LRD can be characterized by  
 459 evaluating the scaling exponent  $H$  (or Hurst coefficient) of a self-similar process. When plotted  
 460 on a log/log plot, the resulting slope of the best fit line gives an estimate of  $H$ , where values  
 461 approaching 1.0 indicate dominant long-range effects (see Beran, 1994).

462 For a given number of observations  $X_1, X_2, \dots, X_n$ , a partial sum sequence is defined by  
 463  $S_m = X_1 + \dots + X_m$ , for  $m = 0, 1, \dots$  and  $m < n$  (with  $S_0 = 0$ ). The R/S statistic is then calculated by  
 464 (see Samorodnitsky, 2007):

$$\frac{R}{S}(X_1, \dots, X_n) = \frac{\max_{0 \leq i \leq n} (S_i - \frac{i}{n} S_n) - \min_{0 \leq i \leq n} (S_i - \frac{i}{n} S_n)}{\sqrt{\sum_{i=1}^n (x_i - \frac{i}{n} S_n)^2}}$$

466 (+)  
 467 where,  $S_n/n$  is the mean of the sample. It has been suggested that R/S tends to give biased  
 468 estimates of  $H$ , too low for  $H > 0.72$  and too high for  $H < 0.72$  (Bassingthwaigthe and Raymond,  
 469 1994), which was later confirmed by Malamud and Turcotte (1999). Empirical trend corrections  
 470 to the estimates of  $H$  can be made by graphical interpolation, but are not applied here because of  
 471 how the regression is done. The R/S analysis in this study was performed using signal analysis  
 472 software AutoSignal™ to identify whether a given signal is distinguishable from a random,  
 473 white noise process and, if so, whether the given signal contains LRD. The  $H$  value is calculated  
 474 by an inverse variance-weighted linear least-squares curve fit using the logarithms of the R/S and  
 475 the number of observations, which provides greater accuracy than other programs that compute  
 476 the Hurst coefficient.

477 Two of the simplest statistical time series models that can account for LRD are fGn and  
 478 ARIMA. In the former case, fGn and its “parent” **fractional Brownian motion (fBm)** are used to  
 479 evaluate stationary and nonstationary fractal signals, respectively (see Eke et al., 2000; Everett

Formatted: Default, Left, Indent: First line: 0.5", Space Before: 0 pt, After: 0 pt

Formatted: Default, Indent: First line: 0.5"

**Commented [WB20]: Commented [A20]:** How has this been used in the earth sciences? Provide real world examples to help reader fully understand the application  
**Response:** This comment is similar to the previous comment about including some real world examples and has already been addressed. We deleted equation 1 and the more detailed description of the R/S analysis as this is described in many places and this level of detail is not central to the main discussion on the ARIMA statistical approach. For completeness, we choose to leave the detailed explanation of the ARIMA statistics and equations in the paper, so the reader can see the mathematics described here without having to search the literature.

**Commented [WB21]: Commented [A21]:** What does fBm stand for?  
**Response:** Fixed... fractional Brownian motion



480 and Weiss, 2002). Both fGn and fBm are governed by two parameters: variance  $\sigma^2$ ; and the  
481 scaling parameter,  $H$  (Eke et al., 2000). A more comprehensive class of time series models that  
482 has similar capability to detect long-range structure is ARIMA. Because fGn and fBm models  
483 have only two parameters, it is not possible to model the short-range components. Additional  
484 parameters in ARIMA models are designed to handle the short-range component of the signal, as  
485 discussed by Taqqu et al. (1995) and others. Because the EMI data series presumably contain  
486 both short-range and long-range effects, we chose to use ARIMA as the analyzing technique.

487 ARIMA models are used across a wide range of disciplines in geoscience and have broad  
488 applicability for understanding the statistical structure of a given data series as it is related to  
489 some physical phenomenon (see Beran, 1992, 1994; Box and Jenkins, 1970; Cimino et al., 1999;  
490 Granger and Joyeux, 1980; Hosking, 1981; Taqqu et al., 1995). For example, Cimino et al.  
491 (1999) apply R/S analysis, ARIMA, and Neural Network analysis to different geological data  
492 sets including; tree ring data, Sr isotope data of Phanerozoic seawater samples, and El Niño  
493 phenomenon. The authors show that -their statistical approach enables 1) recognition of  
494 qualitative changes within a given dataset, 2) evaluation of the scale (in)dependency of  
495 increments, 3) characterization of random processes that describe the evolution of the data, and  
496 4) recognition of cycles embedded within the data series. In the soil sciences, Alemi et al. (1988)  
497 use ARIMA and Kriging to model the spatial variation of clay-cover thickness of a 78 km<sup>2</sup> area  
498 in northeast Iran and demonstrate that ARIMA modeling can adequately describe the nature of  
499 the spatial variations. ARIMA models have also been used to model periodicity of major  
500 extinction events in the geologic past (Kitchell and Pena, 1984).

501 In all these studies, <sup>t</sup>The statistical ARIMA model of a given data series is defined by  
502 three terms  $(p,d,q)$ , where  $p$  and  $q$  indicate the order of the autoregressive (AR) and moving  
503 average (MA) components, respectively and  $d$  represents a differencing, or integration term (I)  
504 that is related to LRD. The AR element,  $p$ , represents the effects of adjacent observations and the  
505 MA element,  $q$ , represents the effects on the process of nearby random shocks (Cimino et al.,  
506 1999; De Jong and Penzer, 1998). However, in the present study our series are reversible spatial  
507 series that can be generated, and are identical, with either forward or backward acquisition,  
508 unlike a time series. Both  $p$  and  $q$  parameters are restricted to integer values (e.g., 0, 1, 2),  
509 whereas the integration parameter,  $d$ , represents potentially long-range structure in the data. The

Formatted: Font: Not Bold, Not Italic

Formatted: Font color: Auto

Formatted: Superscript

Formatted: Font color: Auto

510 differencing term  $d$  is normally evaluated before  $p$  and  $q$  to identify whether the process is  
 511 stationary (i.e., constant mean and  $\sigma^2$ ). If the series is nonstationary, it is differenced to remove  
 512 either linear ( $d = 1$ ) or quadratic ( $d = 2$ ) trends, thereby making the mean of the series stationary  
 513 and invertible (Cimino et al., 1999), thus allowing determination of the ARMA  $p$  and  $q$   
 514 parameters.

Formatted: Font color: Red

515 Here, we adopt the definitions of an ARMA  $(p,q)$ , and ARIMA  $(p,d,q)$  process following  
 516 the work of Beran (1994). Let  $p$  and  $q$  be integers, where the corresponding polynomials are  
 517 defined as:

$$518 \quad \phi(x) = 1 - \sum_{j=1}^p \phi_j x^j,$$

$$519 \quad \psi(x) = 1 + \sum_{j=1}^q \psi_j x^j. \tag{12}$$

$$521 \quad \psi(x) = 1 + \sum_{j=1}^q \psi_j x^j.$$

522  
 523 It is important to note that all solutions of  $\phi(x_0) = 0$ , and  $\psi(x) = 0$  are assumed to lie outside  
 524 the unit circle. Additionally, let  $\epsilon_t (t = 1, 2, \dots)$  be independent, and identically distributed  
 525 normal variables with zero variance  $\sigma_\epsilon^2$  such that an ARMA  $(p,q)$  process is defined by the  
 526 stationary solution of:

$$528 \quad \phi(B)X_t = \psi(B)\epsilon_t \tag{23}$$

529  
 530 where,  $B$  is the backward shift operator  $BX_t = X_{t-1}$ ,  $B^2X_t = X_{t-2}$ , ... and, specifically, the  
 531 differences can be expressed in terms of  $B$  as;  $X_t - X_{t-1} = (1 - B)X_t$ ,  $(X_t - X_{t-1}) - (X_{t-1} -$   
 532  $X_{t-2}) = (1 - B)^2X_t$  ... Alternatively, an ARIMA  $(p,d,q)$  process  $X_t$  is formally defined as:

$$534 \quad \phi(B)(1 - B)^d X_t = \psi(B)\epsilon_t \tag{34}$$

535  
 536 where, equation (3) holds for a  $d$ th difference  $(1 - B)^d X_t$ .

537 As mentioned previously, a more general form of ARIMA  $(p,d,q)$  is the fractional  
 538 ARIMA process, or FARIMA, where the differencing term  $d$  is allowed to take on fractional

539 values. If  $d$  is a non-integer value for some  $-0.5 < d < 0.5$  and  $X_t$  is a stationary process as  
540 indicated by equation 34, then the model by definition is called a FARIMA process where  $d$ -  
541 values in the range  $0 < d < 0.5$  are of particular interest herein because geophysically-relevant  
542 LRD occurs for  $0 < d < 0.5$ , whereas  $d > 0.5$  means that the process is nonstationary, but  
543 nonintegrable (Beran, 1994; Hosking, 1981). A special case of a FARIMA process explored in  
544 the current study is ARIMA (0d0), also known as fractionally-differenced white noise (Hosking,  
545 1981), which is defined by Beran (1994) and others as:

546  
547 
$$X_t = (1 - B)^{-d} \epsilon_t.$$

548 (45)

549  
550 For  $0 < d < 0.5$ , the ARIMA (0d0) process is a stationary process with long-range structure and  
551 is useful for modeling LRD. As shown later, different values of the  $d$  parameter provide further  
552 insight into the type of causative physical processes that generate each data series. When  $d < 0.5$ ,  
553 the series  $X_t$  is stationary, which has an infinite moving average MA representation that  
554 highlights long-range trends or cycles in the data. Conversely, when  $d > -0.5$ , the series  $X_t$  is  
555 invertible and has an infinite autoregressive AR representation (see Hosking, 1981). When  $-0.5 <$   
556  $d < 0$ , the stationary, and invertible, ARIMA (0d0) process is dominated by short-range effects  
557 and is antipersistent. When  $d = 0$ , the ARIMA (000) process is white noise, having zero  
558 correlations and a constant spectral density.

559 ~~Following the methodology proposed by Box and Jenkins (1970), there are three phases that~~  
560 ~~characterize ARIMA modeling: identification, estimation, and diagnostic testing. The primary~~  
561 ~~task of the first phase is to identify the autocorrelation function(s) and any patterns in the data~~  
562 ~~(e.g., autocorrelation function, R/S analysis), and to manipulate the data (if necessary) to achieve~~  
563 ~~stationarity before an appropriate model is chosen (Linden et al., 2003). After an appropriate~~  
564 ~~model is selected (e.g., ARMA, ARIMA, etc.), statistical software is used in the second phase to~~  
565 ~~generate estimates of each model parameter ( $p, d, q$ ) in order to achieve a good model fit. Tasks~~  
566 ~~included in the third phase involve examining the residual score, or root-mean-square error~~  
567 ~~(RMSE), to determine if there are patterns remaining in the data that are not accounted for.~~  
568 ~~Residual scores, or the mismatch between the values predicted by the model and the actual~~

Formatted: Indent: First line: 0"

569 values of the data series, should show that there are no significant autocorrelations among the  
570 residuals (Linden et al., 2003). The best model fit is determined by the smallest residual score,  
571 which is the sum of the squares of the residuals (i.e., RMSE).

572 Identification of an appropriate model is accomplished by finding small values of elements  $p, d, q$   
573 (usually between 0 – 2) that accurately fit the most significant patterns in the data series. When a  
574 value of an element is 0, that element is not needed. For example, if  $d = 0$  the series does not  
575 contain a significant long-range component, whereas if  $p = q = 0$ , the model does not exhibit  
576 significant short-range effects. If  $p, d, q \neq 0$ , the model contains a combination of both short and  
577 long-memory effects.

578 Time series modeling is traditionally used for either forecasting future values or assigning  
579 missing values within the data series. In this study, we are interested in determining the orders of  
580  $p, d, q$  not for forecasting or filling in missing data, but rather for gaining physical insight into the  
581 structure of EMI  $\sigma_a$  responses, and since it is a proxy, the structure of the framework geology.  
582 Different combinations of  $(p, d, q)$  provide insights into the degree or strength of LRD within a  
583 data series and, in the present context in which EMI and elevation DEM are jointly analyzed, the  
584 best fit  $(p, d, q)$  values can be used to discern how the various length scales within the framework  
585 geology and island morphology are related.

## 586 4 Results

### 587 4.1 Spatial data series

#### 588 4.1.1 EMI and GPR surveys

590 ~~The 100 km EMI survey (Fig. 2a) represents (to our knowledge) the longest continuous ground-~~  
591 ~~based survey using a terrain conductivity meter ever performed.~~ The unprocessed (raw) EMI  $\sigma_a$   
592 responses show a high degree of variability along the island. ~~To reduce the effect of instrument~~  
593 ~~drift caused by temperature, battery and other systematic variations through the acquisition~~  
594 ~~interval, a drift correction was applied to each segment, the segments were then stitched together,~~  
595 ~~following which a regional linear trend removal was applied to the composite dataset.~~ High-  
596 amplitude responses within the EMI signal generally exhibit a higher degree of variability  
597 (multiplicative noise) compared to the low-amplitude responses. Higher  $\sigma_a$  readings correspond  
598 to a small sensor footprint and have enhanced sensitivity to small-scale near-surface

**Commented [WB22]:** Commented [A22]: Superfluous, and the data are not new to this study.

**Response:** Fixed

**Commented [WB23]:** Commented [A23]: This is Methods, not Results.

**Response:** Fixed... moved to the Methods section (new lines 301-304).

599 heterogeneities (see Guillemoteau and Tronicke, 2015). Low  $\sigma_a$  readings suggest the sensor is  
600 probing greater depths and averaging over a larger footprint. In that case, the effect of fine-scale  
601 heterogeneities that contribute to signal variability is suppressed.

602 The 10 km alongshore survey is located within an inferred paleo-channel region (Fisk,  
603 1959), providing some *a priori* geologic constraints for understanding the variability within the  
604 EMI signal (Fig. 2b). Here, the sample size is  $n = 10,176$ , permitting a quantitative comparison  
605 with the 100-km-long data series since they contain a similar number of observations. Unlike the  
606 100 km survey, successive footprints of the sensor at each subsequent measurement point  
607 overlap along the 10 km survey. The overlap enables a fine-scale characterization of the  
608 underlying geological structure because the separation between the TX – RX coils (1.21 m), a  
609 good lower-bound approximation of the footprint, is greater than the step-size (1 m).

610 The overall trend in  $\sigma_a$  for the 10 km survey is comparable to that of the 100 km survey,  
611 where regions characterized by high and low amplitude signals correspond to regions of high and  
612 low variability, respectively, implying that multiplicative noise persists independently of station  
613 spacing. The decrease in  $\sigma_a$  that persists between  $\sim 2.5 - 6$  km along the profile (Fig. 2b)  
614 coincides in location with two paleo-channels, whereas a sharp reduction in  $\sigma_a$  is observed at  $\sim$   
615 8.2 km in close proximity to a smaller channel. Most of the known paleo-channels are located  
616 within the 10 km transect and likely contain resistive infill sands that should generate lower and  
617 relatively consistent  $\sigma_a$  readings (Weymer et al., 2015a). The low  $\sigma_a$  signal caused by the sand  
618 indirectly indicates valley incision, since it is diagnostic of a thicker sand section, relatively  
619 unaffected by the underlying conductive layers. Thus, it is reasonable to assume that reduced  
620 variability in the signal is related to the framework geology within the paleo-channels, which we  
621 now compare with a GPR profile.

622 To corroborate the capability of the EMI data to respond to the variable subsurface  
623 geology, an 800 m GPR survey confirms the location of a previously identified paleo-channel  
624 (Fisk, 1959) at  $\sim 5 - 10$  m depth (Fig. 3). A continuous undulating reflector from  $\sim 150 - 800$  m  
625 along the profile is interpreted to be the surface mapped by Fisk (1959) who documented a  
626 paleo-channel at this location with a depth of  $\sim 8$  m. Although the paleo-surface is within the  
627 detection limits of the GPR, it is likely that the DOI of the EMI data ( $\sim 3 - 6$  m) is not large  
628 enough to probe continuously along the contact between the more conductive ravinement surface

**Commented [WB24]:** Commented [A24]: Draw this interpretation on the GPR data in Fig 3.

**Response:** Fixed (see revised Figure 3 in the rebuttal letter).

629 and the moreless resistive infill sands. Along the transect at shallower depths highlighted by the  
630 red box in the lower radargram (Fig. 3), low EMI  $\sigma_a$  values correspond to fine stratifications in  
631 the GPR section, which is common for beach sands with little clay content that are not saline-  
632 saturated. The EMI highs between ~ 450 – 530 m coincide with parts of the GPR section that do  
633 not have the fine stratification and this may indicate the presence of clay or saline water. Here,  
634 the high conductivity zone for both the GPR and EMI is located within a recovering washover  
635 channel overlying the paleo-channel that is evident in the satellite imagery in the upper-left panel  
636 of Fig. 3. The overwash deposits consisting of a mix of sand and finer-grained backbarrier  
637 sediments likely mask the EMI sensors' ability to probe greater depths. Nonetheless, the high  
638 conductivity zone represents a smaller ~ 100 m segment within the ~ 500-m-wide paleo-channel,  
639 suggesting that variations in the EMI responses outside this zone are directly related to variations  
640 in the framework geology imaged by GPR.

641

#### 642 4.1.2 LiDAR-derived DEM morphometrics

643 The LiDAR-derived elevation DEM spatial data series along the 100 km transect are presented in  
644 Fig. 4. Each data series is shown with respect to the areal DEM of the study area where the  
645 approximate locations of each closely-spaced paleo-channel are highlighted in gray. This  
646 visualization allows a qualitative analysis of the spatial relationships between paleo-channels,  
647 subsurface information encoded in the  $\sigma_a$  signal, and surface morphology over the entire length  
648 of the barrier island.

649 The morphology of the beach-dune system, as well as island width, changes substantially  
650 from north to south. In the paleo-channel region, beach width decreases considerably in the  
651 central channel (~ 37 – 42 km) and is more variable outside this region. Beach width generally  
652 increases towards the northern section of the island. The volume of the beach tends to be lowest  
653 in the northern zone, varies considerably in the central part of the island, then stabilizes and  
654 gradually decreases towards the south. These zones correspond to the southern (0 – 30 km),  
655 central (30 – 60 km), and northern (60 – 100 km) sections of the island. Alongshore dune heights  
656 generally are greater in the south, become slightly more variable in the paleo-channel region, and  
657 decrease in the north except for the area adjacent to Baffin Bay. Dune volume is lowest in the  
658 northern section, intermittently increases in the central zone and slightly decreases towards the

**Commented [WB25]:** Commented [A25]: This is very subtle and may be only true for the central channel.

**Response:** Fixed

**Commented [WB26]:** Commented [A26]: Again, this appears to be very subtle

**Response:** Fixed

659 south. The island is considerably narrower between Mansfield Channel and Baffin Bay (see Fig.  
660 2a), increasing in width ~~significantly~~ in the northern zone; island volume follows a similar trend.  
661 Overall,  $\sigma_a$  values are lower northward of the paleo-channel region compared to the southern  
662 zone where  $\sigma_a$  increases substantially. However, the lowest  $\sigma_a$  values are located within the  
663 region of paleo-channels inferred by Fisk (1959) supporting previous findings in the study area  
664 by Weymer et al. (2015a) and Wernette et al. (2018) that suggest a potential geologic control on  
665 alongshore geomorphic features.

666 Each spatial data series (Fig. 4a – 4g) represents a different superposition of effects  
667 caused by physical processes operating across a wide range of temporal and length scales  
668 (Weymer et al., 2015a). Short-range fluctuations represent small-scale heterogeneities, whereas  
669 long-range components capture variations in each metric at broader length scales. There is a high  
670 degree of variability within each signal that is directly related to the ~~complex~~ geological and  
671 geomorphological structure along the island. Within and outside the paleo-channel region,  
672 general associations between ~~the~~ EMI  $\sigma_a$  responses and DEM metrics ~~are visually subtle can be~~  
673 ~~made, motivating the statistics as~~ we now show by ARIMA modeling. To conduct the ARIMA  
674 analysis, we chose to divide the island into three zones based on the location of the known paleo-  
675 channels. As will be discussed later, the tripartite zonation allows for a quantitative analysis of  
676 LRD at three spatial scales (regional, intermediate, local) within and outside the area containing  
677 paleo-channels. It is important to note, however, that the framework geology is likely to exhibit  
678 LRD regardless of the length-scale over which it is observed.

## 679 4.2 Tests for LRD

### 680 4.2.1 Tests for LRD in EMI data series

681 Both EMI spatial data series appear to be nonstationary since the mean and variance of the data  
682 fluctuate along the profile. A closer visual inspection reveals however that cyclicity is present at  
683 nearly all spatial frequencies (Fig. 6), with the cycles superimposed in random sequence and  
684 added to a constant variance and mean (see Beran, 1994). This behavior is typical for stationary  
685 processes with LRD, and is often observed in various types of geophysical time series (Beran,  
686 1992), for example records of Nile River stage minima (Hurst, 1951). A common first-order  
687 approach for determining whether a data series contains LRD is through inspection of the  
688

**Commented [WB27]:** Commented [A27]: This is statistically significant?

**Response:** No, not statistically significant. Deleted 'significantly' to avoid confusion.

**Commented [WB28]:** Commented [A28]: Didn't Wernette et al, 2018 show this as well?

**Response:** Yes, added Wernette et al. (2018)

**Commented [WB29]:** Commented [A29]: Why is a barrier island with 3 paleochannels complex?

**Response:** deleted 'complex'

**Commented [WB30]:** Commented [A30]: Better to call out that the associations are visibly subtle so you're going to apply statistics to demonstrate it.

**Response:** Fixed

**Commented [WB31]:** Commented [A31]: Can the reader see this? Figure?

**Response:** Fixed. Added a ref to Fig. 6



689 autocorrelation function, which we have computed in AutoSignal™ signal analysis software  
690 using a fast Fourier transform (FFT) algorithm (Fig. 5a, 5d). Both EMI signals exhibit large  
691 correlations at large lags (at km and higher scales), suggesting the  $\sigma_a$  responses contain LRD, or  
692 "long-memory effects" in time-series language. ~~The degree of LRD can be characterized by~~  
693 ~~evaluating the scaling exponent  $H$  (or Hurst coefficient) of a self-similar process. When plotted~~  
694 ~~on a log/log plot, the resulting slope of the best-fit line gives an estimate of  $H$ , where values~~  
695 ~~approaching 1.0 indicate dominant long-range effects (see Beran, 1994).~~ Results from a rescaled  
696 range  $R/S$  analysis (Fig. 5b, 5e) indeed show high  $H$ -values of 0.85 ( $r^2 = 0.98$ ) and 0.95 ( $r^2 =$   
697 0.99) for the 100 km and 10 km surveys, indicating a strong presence of LRD at both regional  
698 and local spatial scales.

699 The manner in which different spatial frequency (i.e. wavenumber) components are  
700 superposed to constitute an observed EMI  $\sigma_a$  signal has been suggested to reveal information  
701 about the causative multi-scale geologic structure (Everett and Weiss, 2002; Weymer et al.,  
702 2015a). For example, the lowest-wavenumber contributions are associated with spatially  
703 coherent geologic features that span the longest length scales probed. The relative contributions  
704 of the various wavenumber components can be examined by plotting the  $\sigma_a$  signal power spectral  
705 density (PSD). A power-law of the form  $|\sigma_a(f)|^2 \sim f^\beta$  over several decades in spatial wavenumber  
706 is evident (Fig. 5c, 5f). The slope  $\beta$  of a power-law-shaped spectral density provides a  
707 quantitative measure of the LRD embedded in a data series and characterizes the heterogeneity,  
708 or "roughness" of the signal. A value of  $|\beta| > 1$  indicates a series that is influenced more by  
709 long-range correlations and less by small-scale fluctuations (Everett and Weiss, 2002). For  
710 comparison, a pure white noise process would have a slope of exactly  $\beta = 0$ , whereas a slope of  $\beta$   
711  $\sim 0.5$  indicates fractional Gaussian noise, i.e., a stationary signal with no significant long-range  
712 correlations (Everett and Weiss, 2002). The  $\beta$ -values for the 100 km and 10 km surveys are  $\beta = -$   
713 0.97, and  $\beta = -1.06$ , respectively. These results suggest that both the 100 km and 10 km EMI  
714 signals contain long-range correlations. However, there is a slightly stronger presence of LRD  
715 within the 10 km segment of the paleo-channel region compared to that within the segment that  
716 spans the entire length of the island. This indicates that long-range spatial variations in the  
717 framework geology are more important, albeit marginally so, at the 10-km scale than at the 100-  
718 km scale. It is possible that the variability within the signal and the degree of long-range

719 correlation is also a function of the sensor footprint, relative to station spacing. This is critically  
720 examined in section 4.3.

721

#### 722 4.2.2 Tests for LRD in surface morphometrics

723 Following the same procedure as applied to the EMI data, we performed the R/S analysis for  
724 each beach, dune, and island metric. The calculated  $H$ -values for the DEM morphometrics range  
725 between 0.80 – 0.95 with large values of  $r^2 \sim 1$ , indicating varying, but relatively strong  
726 tendencies towards LRD. Beach width and beach volume data series have  $H$ -values of 0.82 and  
727 0.86, respectively. Dune height and dune volume  $H$ -values are 0.83 and 0.80, whereas island  
728 width and island volume have higher  $H$ -values of 0.95 and 0.92, respectively. Because each data  
729 series shows moderate to strong evidence of LRD, the relative contributions of short and long-  
730 range structure contained within each signal can be further investigated by fitting ARIMA  
731 models to each data set.

732

#### 733 4.3 ARIMA statistical modeling of EMI

734 The results of the tests described in section 4.2.1 for estimating the self-similarity parameter  $H$   
735 and the slope of the PSD function suggest that both EMI data series, and by inference the  
736 underlying framework geology, exhibit LRD. ~~Therefore, we suggest that an ARIMA process~~  
737 ~~might be an appropriate model.~~ The goal of our analysis using ARIMA is to estimate the  $p$ ,  $d$ ,  
738 and  $q$  terms representing the order, respectively, of autoregressive (AR), integrated (I) and  
739 moving-average (MA) contributions to the signal (Box and Jenkins, 1970) to quantify free vs.  
740 forced behavior along the island. For the analysis, the ‘arfirm’ and ‘forecast’ statistical packages  
741 in R were used to fit a family of ARIMA ( $p,d,q$ ) models to the EMI  $\sigma_a$  data and island  
742 morphometrics (Hyndman, 2015; Hyndman and Khandakar, 2007; Veenstra, 2012). Results of  
743 ten realizations drawn from a family of ARIMA ( $p,d,q$ ) models and their residuals (RMSE) are  
744 presented in Table 1. The worst fit (ARIMA 001) models are shown for the 100 km and 10 km  
745 (Fig. 6a, 6c) surveys. The best fit (ARIMA 0d0) models for both the 100 and 10 km surveys are  
746 shown in Fig. 6b and 6d, respectively. For this analysis, the tests include different combinations  
747 of  $p,d,q$  that model either short-range: ARIMA (100; 001; 101; 202; 303; 404; 505), long-range:  
748 ARIMA (010; 0d0), or composite short- and long-range processes: ARIMA (111). It is important

**Commented [WB32]:** Commented [A32]: Why, more explicitly? The justification should be in the Methods or Intro sections, not here.

**Response:** We agree and deleted this sentence as we already discuss this in the Methods section

**Commented [WB33]:** Commented [A33]: In order to do what?

**Response:** We are doing this to quantify free vs. forced behavior and added this statement for clarification.

749 to note that AR and MA are only appropriate for “short-memory” processes since they involve  
750 only near-neighbor values to explain the current value, whereas the integration (the "I" term in  
751 ARIMA) models “long-memory” effects because it involves distant values. Note that ARIMA  
752 was developed for one-way time series, in which the arrow of time advances in only one  
753 direction, but in the current study we are using it for spatial series that are reversible. Different  
754 realizations of each ARIMA ( $p,d,q$ ) data series were evaluated, enabling physical interpretations  
755 of LRD at regional, intermediate, and local spatial scales. Determining the best-fitting model is  
756 achieved by comparing the residual score, or RMSE, of each predicted data series relative to the  
757 observed data series, where lower RMSE values indicate a better fit (Table 1).

758         Based on the residuals and visual inspection of each realization (Fig. 6), two observations  
759 are apparent: 1) both EMI data series are most accurately modeled by an ARIMA ( $0d0$ ) process  
760 with non-integer  $d$ , and 2) the mismatch between the data and their model fit is considerably  
761 lower for the 10 km survey compared to the 100 km survey. The first observation suggests that  
762 the data are most appropriately modeled by a FARIMA process; i.e., a fractional integration that  
763 is stationary ( $0 < d < 0.5$ ) and has long-range dependence (see Hosking, 1981). This implies that  
764 spatial variations in framework geology at the broadest scales dominate the EMI signal and that  
765 small-scale fluctuations in  $\sigma_a$  caused, for example, by changing hydrological conditions over  
766 brief time intervals less than the overall data acquisition interval, or fine-scale lithological  
767 variations less than a few station spacings, are not as statistically significant. Regarding the  
768 second observation, the results suggest that a small station spacing (i.e., 1 m) is preferred to  
769 accurately model both short and long-range contributions within the signal because large station  
770 spacings cannot capture short-range information. The model for the 10 km survey fits better  
771 because both  $p$  (AR) and  $q$  (MA) components increase with a smaller step-size since successive  
772 volumes of sampled subsurface overlap. On the contrary, the sensor footprint is considerably  
773 smaller than the station spacing (10 m) for the 100 km survey. Each  $\sigma_a$  measurement in that case  
774 records an independent volume of ground, yet the dataset still exhibits LRD, albeit not to the  
775 same degree as in the 10 km survey.

776

777 4.4 ARIMA statistical modeling of island metrics compared with EMI

778 A sequence of ARIMA ( $p,d,q$ ) models was also evaluated for the ~~elevation~~DEM morphometrics  
779 series to find best fits to the data. The analysis comprised a total of 36 model tests (Table 2). The  
780 RMSE values reveal that: 1) all data series are best fit by an ARIMA ( $0d0$ ) process with  
781 fractional  $d$ , i.e. a FARIMA process; 2) the ARIMA models, in general, more accurately fit the  
782 EMI data than the DEM morphometric data likely because the morphology is controlled by more  
783 than the framework geology alone; and 3) in all cases, the poorest fit to each series is the  
784 ARIMA (001), or MA process. This, in turn, means that the differencing parameter  $d$  is the most  
785 significant parameter amongst  $p$ ,  $d$  and  $q$ . It is important to note that different values of  $d$  were  
786 computed based on the best fit of each FARIMA model to the real data. A graphical  
787 representation of the FARIMA-modeled data series for each DEM metric is shown in Fig. 7,  
788 allowing a visual inspection of how well the models fit the observed data. Because each data  
789 series has its own characteristic amplitude and variability, it is not possible to compare RMSE  
790 between tests without normalization. The variance within each data series can differ by several  
791 orders of magnitude.

792 Instead of normalizing the data, a fundamentally different approach is to compare the  
793 EMI  $\sigma_a$   $d$ -values with respect to each metric at regional, intermediate, and local scales (Table 3).  
794 Higher positive  $d$ -values indicate of a stronger tendency towards LRD. According to Hosking  
795 (1981),  $\{x_t\}$  is called an ARIMA ( $0d0$ ) process and is of particular interest in modelling LRD as  
796  $d$  approaches 0.5 because in such cases the correlations and partial correlations of  $\{x_t\}$  are all  
797 positive and decay slowly towards zero as the lag increases, while the spectral density of  $\{x_t\}$  is  
798 concentrated at low frequencies. It is reasonable to assume that the degree of LRD may change  
799 over smaller intermediate and/or local scales, which implies a breakdown of self-similarity. For a  
800 self-similar signal,  $d$  is a global parameter that does not depend on which segment of the series is  
801 analyzed. In other words, the  $d$ -values should be the same at all scales for a self-similar structure.

802 The results of the FARIMA analysis at the intermediate scale vary considerably within  
803 each zone of the barrier island (north, central, south) and for each spatial data series (Table 3). In  
804 the southern zone (0 – 30 km), EMI  $\sigma_a$  and beach volume have the strongest LRD ( $d = 0.44$ ),  
805 whereas the other metrics exhibit weak LRD (ranging from  $d \sim 0 - 0.2$ ), which may be  
806 characterized approximately as a white noise process. Within the paleo-channel region (30 – 60  
807 km), all of the island metrics show a moderate to strong tendency towards LRD ( $0.3 \leq d \leq 4.2$ ),

**Commented [WB34]:** Commented [A34]: Likely because the morphology is controlled by more than framework geology.

**Response:** We agree and added this statement to the sentence as suggested by the Reviewer.

808 however, the EMI signal does not ( $d = 0.11$ ). In the northern zone (60 – 100 km) all data series  
809 contain moderate to strong LRD with the exception of beach and island width.

810 A FARIMA analysis was also conducted at the local scale by dividing the island into 10-  
811 km-segments, starting at the southern zone (0 – 10 km) and ending at the northern zone of the  
812 island (90 – 100 km). A total of 70 FARIMA model realizations were evaluated and the resulting  
813  $d$ -values demonstrate that the EMI data segments show a stronger presence of LRD ( $d > 0.4$ )  
814 within the paleo-channels (30 – 60 km) and further to the north (60 – 80 km) in close proximity  
815 to the ancestral outlet of Baffin Bay. These findings indicate that there may be local and/or  
816 intermediate geologic controls along different parts of the island, but that the framework geology  
817 dominates island metrics at the regional scale.

818

## 819 5 Discussion

820 Although it has long been known that processes acting across multiple temporal and length  
821 scales permit the shape of coastlines to be described by mathematical constructs such as power  
822 law spectra and fractal dimension (Lazarus et al., 2011; Mandelbrot, 1967; Tebbens et al., 2002),  
823 analogous studies of the subsurface framework geology of a barrier island have not been carried  
824 out. ~~For the first time, it is-~~ This research supports previous studies demonstrating ed-that near-  
825 surface EMI geophysical methods are useful for mapping barrier island framework geology and  
826 that FARIMA data series analysis is ~~useful-~~ a compact statistical tool for illuminating the long  
827 ~~and/or short-range~~ spatial correlations~~connections~~ between subsurface geology and  
828 geomorphology. The results of the FARIMA analysis and comparisons of the best-fitting  $d$ -  
829 parameters show that beach and dune metrics closely match EMI  $\sigma_a$  responses *regionally* along  
830 the entire length of PAIS, suggesting that the long-range dependent structure of these data series  
831 is similar at large spatial scales. However, further evaluation of the  $d$ -parameters over smaller  
832 data segments reveals that there are ~~additional intermediate and~~ localized framework geology  
833 controls on island geomorphology that are not present at the regional scale.

834 At the *intermediate* scale, a low EMI  $d$ -value ( $d = 0.11$ ) suggests there is only a weak  
835 framework-geologic control on barrier island morphometrics. A possible explanation is that the  
836 paleo-channels, located within a ~ 30 km segment of the island, are not regularly spaced and on  
837 average are less than a few km wide. This implies that the framework geology controls are

**Commented [WB35]: Commented [A35]:** There are a number of recent papers that have already demonstrated this. This research supports previous papers but has been shown already in recent papers.

**Response:** Yes, we agree with the Reviewer and changed this sentence to state that the current study supports our previous research.

**Commented [WB36]: Commented [A36]:** Seems like a fair amount of complex statistics to just be useful; why are the methods chosen the best for testing the hypothesis?

**Response:** We deleted 'useful' and changed to state that FARIMA is a compact statistical tool that is designed to handle both short and long-range correlations that other statistical models do not account for.

**Commented [WB37]: Commented [A37]:** It's possible that at smaller scales, processes driving change are more important

**Response:** Changed this statement to focus on the 'localized' framework geology controls.

**Commented [WB38]: Commented [A38]:** The 2 sentences appear contradictory

**Response:** We changed the previous sentence to avoid any contradictory statements regarding the possible local framework geology controls.

838 **localized** (i.e., effective in shaping island geomorphology only at smaller spatial scales). At the  
839 *local* scale, relationships between the long-range-dependence of EMI and each metric vary  
840 considerably, but there is a significant geologic control on dune height within the paleo-channel  
841 region ( $d > 0.4$ ). It is hypothesized that the alongshore projection of the geometry of each  
842 channel is directly related to a corresponding variation in the EMI signal, such that large, gradual  
843 minima in  $\sigma_a$  are indicative of large, deep channel cross-sections and small, abrupt minima in  $\sigma_a$   
844 represent smaller, shallow channel cross-sections. At shallower depths within the DOI probed by  
845 the EMI sensor, variability in the  $\sigma_a$  signal may correspond to changes in sediment characteristics  
846 as imaged by GPR (Fig. 3). Located beneath a washover channel, a zone of high conductivity  
847 EMI  $\sigma_a$  responses between  $\sim 450 - 530$  m coincides with a segment of the GPR section where  
848 the signal is more attenuated and lacks the fine stratification that correlates much better with the  
849 lower  $\sigma_a$  zones. The contrasts in lithology between the overwash deposits and stratified infilled  
850 sands was detected by both EMI and GPR measurements, **suggesting that EMI is a useful tool for**  
851 **mapping variations in barrier island framework geology.**

852 It is argued herein that differences in the  $d$  parameter between EMI  $\sigma_a$  readings (our  
853 assumed proxy for framework geology) and LiDAR-derived surface morphometrics provide a  
854 new metric that is useful for quantifying the causative physical processes that govern island  
855 transgression across multiple spatial scales. All of the calculated  $d$ -values in this study are  
856 derived from ARIMA ( $0d0$ ) models that fit the observations, and lie within the range of  $0 < d <$   
857  $0.5$ , suggesting that each data series is stationary but does contain long-range structure that  
858 represents randomly-placed cyclicities in the data. For all models in our study, the  $d$ -values range  
859 between ( $\sim 0 - 0.50$ ), which enables a geomorphological interpretation of the degree of LRD and  
860 self-similarity at different spatial scales. In other words, the  $d$ -parameter not only provides an  
861 indication of the scale dependencies within the data, **but also offers a compact way for analyzing**  
862 **the statistical connections between free (weaker  $d \sim 0$ ) or forced (stronger  $d \sim 0.5$ ) and free**  
863 **(weaker  $d \sim 0$ ) behavior that may be more influenced by morphodynamic processes operating at**  
864 **smaller spatial scales geomorphological evolution along the island.**

865 Alongshore variations in beach width and dune height are not uniform ~~at~~ PAIS and exhibit  
866 different spatial structure within and outside the paleo-channel region (Fig. 5). These  
867 dissimilarities may be forced by the framework geology within the central zone of the island but

**Commented [WB39]:** Commented [A39]: It's not clear why? Does it instead imply that framework geo doesn't have any control at this scale?

**Response:** Yes, what we mean here is that there no framework geology controls at the intermediate scale, and that instead they are more localized within the paleo-channels.

**Commented [WB40]:** Commented [A40]: This has already been shown in previous publications and does not need to be repeated herein.

**Response:** Fixed... deleted.

**Commented [WB41]:** Commented [A41]: What if the geomorphology is more influenced by hydrodynamics at this scale?

**Response:** Fixed. We added this comment by the Reviewer for clarification.

**Formatted:** Line spacing: 1.5 lines

868 are influenced more by contemporary morphodynamic processes outside the paleo-channel  
869 region. ~~Once the dunes are initialized in part by the framework geology, stabilizing vegetation~~  
870 ~~may act as another important control on beach-dune evolution alongshore (Hesp, 1988).~~ This  
871 effect could be represented by higher-wavenumber components embedded within the spatial data  
872 series. Beach and dune morphology in areas that are not controlled by framework geology (e.g.,  
873 the northern and southern zones) exhibit more small-scale fluctuations representing a free system  
874 primarily controlled by contemporary morphodynamics (e.g., wave action, storm surge, wind,  
875 etc.).

876 Because variations in dune height exert an important control on storm impacts (Sallenger,  
877 2000) and ultimately large-scale island transgression (Houser, 2012), ~~it is argued here that the~~  
878 ~~framework geology (or lack thereof) of PAIS acts as an important control on island response to~~  
879 ~~storms and sea-level rise. This study supports recent work by Wernette et al. (2018) suggesting~~  
880 ~~that framework geology can influence barrier island geomorphology by creating alongshore~~  
881 ~~variations in either oceanographic forcing and/or sediment supply and texture that controls~~  
882 ~~smaller-scale processes responsible for beach-dune interaction at the local scale. The forced~~  
883 ~~behavior within the paleo-channel region challenges existing shoreline change studies - models~~  
884 ~~that consider only small-scale undulations in the dune line that are caused by natural randomness~~  
885 ~~within the system. Rather, we propose that dune growth is forced by the framework geology,~~  
886 whose depth is related to the thickness of the modern shoreface sands beneath the beach. This  
887 depth is the primary quantity that is detected by the EMI sensor. With respect to shoreline  
888 change investigations, improving model performance requires further study of how the  
889 framework geology influences beach-dune morphology through variations in wave energy,  
890 texture, and sediment supply (e.g., Houser, 2012; McNinch, 2004; Schwab et al., 2013).

891 Our findings extend previous framework geology studies from the Outer Banks, NC (e.g.,  
892 Browder and McNinch, 2006; McNinch, 2004; Riggs et al., 1995; Schupp et al., 2006), Fire  
893 Island, NY (e.g., Hapke et al., 2010; Lentz and Hapke, 2011), and Pensacola, FL (e.g., Houser,  
894 2012) where feedbacks between geologic features and relict sediments within the littoral system  
895 have been shown to act as an important control on dune growth and evolution. Nonetheless, most  
896 of these studies focus on offshore controls on shoreface and/or beach-dune dynamics at either  
897 local or intermediate scales because few islands worldwide exist that are as long and/or

**Commented [WB42]:** Commented [A42]: Not convinced this has been demonstrated by the analysis.

**Response:** We agree with the Reviewer and deleted this statement as this is a concept better explained in Houser et al. (2018) and Wernette et al. (2018).

**Formatted:** Don't adjust space between Latin and Asian text, Don't adjust space between Asian text and numbers

**Commented [WB43]:** Commented [A43]: Or lack of framework geo

**Response:** Fixed. Added (or lack thereof)...

**Commented [WB44]:** Commented [A45]: Which existing models?

**Response:** We are referring to shoreline change studies that do not include the variable framework geology. For clarification, we added a sentence suggesting that the framework geology needs to be included to improve model performance and added few citations as examples.

**Commented [WB45]:** Commented [A44]: This needs to be better developed. A discussion on how the framework geology interacts with the processes driving change that will result in differing responses would be helpful.

**Response:** We agree with the reviewer and added the following discussion citing Wernette et al. (2018) that describes this concept in greater detail.

898 continuous as North Padre Island. To our knowledge, few framework geology studies have  
899 specifically used statistical testing to analyze correlations between subsurface geologic features  
900 and surface morphology. Two notable exceptions include Browder and McNinch (2006), and  
901 Schupp et al. (2006), both of which used chi-squared testing and cross-correlation analysis to  
902 quantify the spatial relationships between offshore bars, gravel beds, and/or paleo-channels at the  
903 Outer Banks, NC. Although these techniques are useful for determining spatial correlations  
904 between different data sets, they do not provide information about the scale (in)dependencies  
905 between the framework geology and surface geomorphology that FARIMA models are better  
906 designed to handle. The current study augments the existing literature in that 1) it outlines a  
907 quantitative method for determining *free* and *forced* evolution of barrier island geomorphology at  
908 multiple length scales, and 2) it demonstrates that there is a first-order control on dune height at  
909 the local scale within an area of known paleo-channels, suggesting that framework geology  
910 controls are localized within certain zones of PAIS.

911 Further study is required to determine how this combination of free- and forced-behavior  
912 resulting from the variable and localized framework geology affects island transgression.  
913 Methods of data analysis that would complement the techniques presented in this paper might  
914 include; ~~spatiotemporal modeling,~~ power spectral analysis, wavelet decomposition, and shoreline  
915 change analysis that implicitly includes variable framework geology, ~~bicoherence analysis, and~~  
916 ~~wavelet coherence.~~ These approaches would provide important information regarding: 1)  
917 1.——Coherence and phase relationships between subsurface structure and island  
918 geomorphology, and 2)  
919 2.——Non-linear interactions of coastal processes across large and small spatiotemporal  
920 scales.

921 Quantifying and interpreting the significance of framework geology as a driver of barrier  
922 island formation and evolution and its interaction with contemporary morphodynamic processes  
923 is essential for designing and sustainably managing resilient coastal communities and habitats.

## 924 6 Conclusions

926 This study demonstrates the utility of EMI geophysical profiling as a new tool for mapping the  
927 length-scale dependence of barrier island framework geology and introduces the

**Commented [WB46]:** Commented [A46]: This was done by Wernette et al, 2018

**Response:** Ok, deleted and added a statement suggesting that future work is needed to model shoreline change that includes the variable framework geology.

**Formatted:** Normal, Indent: First line: 0.5", No bullets or numbering

**Formatted:** Indent: First line: 0.5"



928 ~~potential importance of statistical modeling of geophysical and geomorphological spatial data~~  
 929 ~~series by FARIMA analysis to better understand the geologic controls on large-scale barrier~~  
 930 ~~island transgression.~~ The EMI and morphometric data series exhibit LRD to varying degrees, and  
 931 each can be accurately modeled using a non-integral parameter  $d$ . The value of this parameter  
 932 diagnoses the spatial relationship between the framework geology and surface geomorphology.  
 933 At the *regional scale* (~100 km), small differences in  $d$  between the EMI and morphometrics  
 934 series suggest that the long-range-dependent structure of each data series with respect to EMI  $\sigma_a$   
 935 is statistically similar. At the *intermediate scale* (~30 km), there is a greater difference between  
 936 the  $d$ -values of the EMI and island metrics within the known paleo-channel region, suggesting a  
 937 more localized geologic control with less contributions from broader-scale geological structures.  
 938 At the *local scale* (10 km), there is a considerable degree of variability between the  $d$ -values of  
 939 the EMI and each metric. These results all point toward a *forced* barrier-island evolutionary  
 940 behavior within the paleo-channel region transitioning into a *free*, or scale-independent behavior  
 941 dominated by contemporary morphodynamics outside the paleo-channel region. In a free system,  
 942 small-scale undulations in the dune line reinforce natural random processes that occur within the  
 943 beach-dune system and are not influenced by the underlying geologic structure. In a forced system,  
 944 the underlying geologic structure establishes boundary constraints that control how the island evolves  
 945 over time. ~~The results from this study suggest that the framework geology initially controls the~~  
 946 ~~development of the dunes at the local scale within the paleo-channel region.~~ This means that  
 947 barrier island geomorphology at PAIS is forced and scale-dependent, unlike shorelines which  
 948 have been shown at other barrier islands to be scale-independent (Tebbens et al., 2002; Lazarus  
 949 et al., 2011). ~~Our findings reveal that shorelines may have different irregularity than island~~  
 950 ~~geomorphology, which suggests an alongshore redistribution of sediment that shapes the~~  
 951 ~~shoreline toward a more dissipative state over time. Without local variations in the framework~~  
 952 ~~geology alongshore, small-scale variations in the shoreline will be masked by the large-scale~~  
 953 ~~transport gradients over long timescales.~~ The exchange of sediment amongst nearshore, beach  
 954 and dune in areas outside the paleo-channel region is scale independent, meaning that barrier  
 955 islands like PAIS exhibit a combination of free and forced behaviors that will affect the response  
 956 of the island to sea level rise and storms. We propose that our analysis is not limited to PAIS but

**Commented [WB47]: Commented [A47]:** Is it the importance of FARIMA or does it demonstrate the potential to use FARIMA for some applications?

**Response:** Fixed. We are suggesting the potential of using FARIMA to understand the statistical connections between surface geomorphology and framework geology.

**Commented [WB48]: Commented [A48]:** The paper would benefit from a discussion of other methods to resolve geologic controls and why FARIMA was best, was chosen.

**Response:** We added a short discussion towards the end of the Discussion section that summarizes the use of other statistical methods to analyze the correlations between framework geology and geomorphology, namely two companion studies by Browder and McNinch, 2006 and Schupp et al., 2006. Please refer to new lines (796-804).

**Formatted:** Font: Italic

**Formatted:** Font: Italic

**Commented [WB49]:** As mentioned previously, this sentence was moved from the Introduction.

**Commented [WB50]: Commented [A49]:** I disagree that it can be stated what initially controlled the formation of dunes from a single elevation model

**Response:** We agree and removed this statement as this is a topic that is explored in more detail by Houser et al. (2018).

**Commented [WB51]:**  
**Commented [A50]:** You didn't study shorelines, correct?

**Response:** Not explicitly, but we were basing this on studies by Lazarus and Tebbens. We deleted this sentence as it is a key argument discussed in Houser et al. 2018 and Wemette et al. (2018) and not explored in the current study.

**Commented [WB52]: Commented [A51]:** This is not a conclusion. It would be appropriate for the Discussion but this analysis did not look at shorelines or sediment transport gradients over time.

**Response:** Fixed. Deleted.

957 can be applied to other barrier islands and potentially in different geomorphic environments, both  
958 coastal and inland.

959

960 **Competing interests.** The authors declare that they have no conflict of interest.

961

962 **Acknowledgments**

963 We are grateful to Patrick Barrineau, Andy Evans, Brianna Hammond Williams, Alex van  
964 Plantinga, and Michael Schwind for their assistance in the field. We thank two anonymous  
965 reviewers for their constructive comments during the open discussion. All data in this study are  
966 available by contacting the corresponding author: brad.weymer@gmail.com. The field data  
967 presented in this manuscript was collected under the National Park Service research permit:  
968 #PAIS-2013-SCI-0005. This research was funded in part by a Grants-in-Aid of Graduate Student  
969 Research Award by the Texas Sea Grant College Program to BW, and through a grant to CH  
970 from the Natural Science and Engineering Research Council of Canada (NSERC).

971

972

973

974

975

976

977

978

979

980

981

982

983

984

985

986

Formatted: Font color: Text 1

Formatted: Font color: Text 1

Formatted: Font color: Text 1

Formatted: Font color: Text 1

987  
988  
989  
990  
991  
992  
993  
994  
995  
996  
997  
998  
999  
1000  
1001  
1002  
1003  
1004  
1005  
1006  
1007  
1008  
1009  
1010  
1011  
1012  
1013  
1014  
1015

**References**

Alemi, M. H., Azari, A. S., and Nielsen, D. R., 1988. Kriging and univariate modeling of a spatially correlated data. Soil technology, 1(2), 133-147.

Anderson, J. B., Wallace, D. J., Simms, A. R., Rodriguez, A. B., Weight, R. W., and Taha, Z. P., 2015. Recycling sediments between source and sink during a eustatic cycle: Systems of late Quaternary northwestern Gulf of Mexico Basin. Earth-Science Reviews 153, 111-138.

Andrle, R., 1996. The west coast of Britain: Statistical self-similarity vs. characteristic scales in the landscape. Earth Surface Processes and Landforms, 21(10), 955-962.

Bailey, R. J., and Smith, D. G., 2005. Quantitative evidence for the fractal nature of the stratigraphic record: results and implications. Proceedings of the Geologists' Association, 116(2), 129-138.

Bassingthwaight, J. B., and Raymond, G. M., 1994. Evaluating rescaled range analysis for time series. Annals of biomedical engineering, 22(4), 432-444.

**Formatted:** English (United States)

**Formatted:** Font: (Default) Times New Roman, 12 pt

**Formatted:** Font: (Default) Times New Roman, 12 pt, Not Italic

**Formatted:** Font: (Default) Times New Roman, 12 pt

**Formatted:** Font: (Default) Times New Roman, 12 pt, Not Italic

**Formatted:** Font: (Default) Times New Roman, 12 pt

1016 Belknap, D. F., and Kraft, J. C., 1985. Influence of antecedent geology on stratigraphic  
1017 preservation potential and evolution of Delaware's barrier systems. *Marine geology*, 63(1),  
1018 235-262.

1019 Beran, J., 1992. Statistical methods for data with long-range dependence. *Statistical Science*, 7(4),  
1020 404-427.

1021 Beran, J., 1994. *Statistics for long-memory processes* (Vol. 61): CRC Press.

1022 Box, G. E., and Jenkins, G. M., 1970. *Time series analysis: forecasting and control* Holden-Day,  
1023 San Francisco, CA.

1024 Browder, A. G., and McNinch, J. E., 2006. Linking framework geology and nearshore morphology:  
1025 correlation of paleo-channels with shore-oblique sandbars and gravel outcrops. *Marine*  
1026 *geology*, 231(1), 141-162.

1027 Brown, L. F., and Macon, J., 1977. *Environmental geologic atlas of the Texas coastal zone:*  
1028 *Kingsville area: Bureau of Economic Geology, University of Texas at Austin.*

1029 Burrough, P., 1981. Fractal dimensions of landscapes and other environmental data. *Nature*,  
1030 294(5838), 240-242.

1031 Buynevich, I. V., FitzGerald, D. M., and van Heteren, S., 2004. Sedimentary records of intense  
1032 storms in Holocene barrier sequences, Maine, USA. *Marine Geology*, 210(1), 135-148.

1033 Cimino, G., Del Duce, G., Kadonaga, L., Rotundo, G., Sisani, A., Stabile, G., . . . Whiticar, M.,  
1034 1999. Time series analysis of geological data. *Chemical Geology*, 161(1), 253-270.

1035 Coleman, J. M., and Gagliano, S. M., 1964. Cyclic sedimentation in the Mississippi River deltaic  
1036 plain.

1037 Colman, S. M., Halka, J. P., Hobbs, C., Mixon, R. B., and Foster, D. S., 1990. Ancient channels  
1038 of the Susquehanna River beneath Chesapeake Bay and the Delmarva Peninsula.  
1039 *Geological Society of America Bulletin*, 102(9), 1268-1279.

1040 Dai, H., Ye, M., & Niedoroda, A. W., 2014. A Model for Simulating Barrier Island  
1041 Geomorphologic Responses to Future Storm and Sea-Level Rise Impacts. *Journal of*  
1042 *Coastal Research*, 31(5), 1091-1102.

1043 De Jong, P., and Penzer, J., 1998. Diagnosing shocks in time series. *Journal of the American*  
1044 *Statistical Association*, 93(442), 796-806.

**Formatted:** Font: (Default) Times New Roman, 12 pt

**Formatted:** Font: (Default) Times New Roman, 12 pt

**Formatted:** Font: (Default) Times New Roman, 12 pt, Not Italic

**Formatted:** Font: (Default) Times New Roman, 12 pt

**Formatted:** Font: (Default) Times New Roman, 12 pt, Not Italic

**Formatted:** Font: (Default) Times New Roman, 12 pt

**Formatted:** Font: 16 pt

- 1045 Delefortrie, S., Saey, T., Van De Vijver, E., De Smedt, P., Missiaen, T., Demerre, I., and Van  
1046 Meirvenne, M., 2014. Frequency domain electromagnetic induction survey in the  
1047 intertidal zone: Limitations of low-induction-number and depth of exploration. *Journal of*  
1048 *Applied Geophysics*, 100, 14-22.
- 1049 Demarest, J. M., and Leatherman, S. P., 1985. Mainland influence on coastal transgression:  
1050 Delmarva Peninsula. *Marine geology*, 63(1), 19-33.
- 1051 Doukhan, P., Oppenheim, G., and Taqqu, M. S., 2003. Theory and applications of long-range  
1052 dependence: Birkhauser.
- 1053 Eke, A., Herman, P., Bassingthwaighite, J., Raymond, G., Percival, D., Cannon, M., . . . Ikrényi,  
1054 C., 2000. Physiological time series: distinguishing fractal noises from motions. *Pflügers*  
1055 *Archiv*, 439(4), 403-415.
- 1056 Evans, M., W, Hine, A., C, Belknap, D., F, and Davis, R., A., 1985. Bedrock controls on barrier  
1057 island development: west-central Florida coast. *Marine geology*, 63(1-4), 263-283.
- 1058 Evans, R. L., and Lizarralde, D., 2011. The competing impacts of geology and groundwater on  
1059 electrical resistivity around Wrightsville Beach, NC. *Continental Shelf Research*, 31(7),  
1060 841-848.
- 1061 Everett, M. E., and Weiss, C. J., 2002. Geological noise in near-surface electromagnetic induction  
1062 data. *Geophysical Research Letters*, 29(1), 10-11-10-14.
- 1063 Everett, M. E., 2013. Near-surface applied geophysics. Cambridge University Press.
- 1064 Fisk, H. N., 1959. Padre Island and Laguna Madre Flats, coastal south Texas. *Proceedings 2nd*  
1065 *Coastal Geography Conference*, Louisiana State University, Baton Rouge, LA, 103-151.
- 1066 Fitterman, D. V., and Stewart, M. T., 1986. Transient electromagnetic sounding for groundwater.  
1067 *Geophysics*, 51(4), 995-1005.
- 1068 Frazier, D. E., 1967. Recent deltaic deposits of the Mississippi River: their development and  
1069 chronology.
- 1070 ~~Geophysical Survey Systems, I. G., 2007. Profiler EMP 400 user's manual, Geophysical Survey~~  
1071 ~~Systems, Incorporated, User's Manual.~~
- 1072 Granger, C. W., and Joyeux, R., 1980. An introduction to long-memory time series models and  
1073 fractional differencing. *Journal of time series analysis*, 1(1), 15-29.

1074 Guillemoteau, J., and Tronicke, J., 2015. Non-standard electromagnetic induction sensor  
1075 configurations: Evaluating sensitivities and applicability. *Journal of Applied Geophysics*,  
1076 118, 15-23.

1077 Gutierrez, B. T., Plant, N. G., Thieler, E. R., and Turecek, A., 2015. Using a Bayesian network to  
1078 predict barrier island geomorphologic characteristics. *Journal of Geophysical Research:*  
1079 *Earth Surface*, 120(12), 2452-2475.

1080 Hapke, C. J., Kratzmann, M. G., and Himmelstoss, E. A., 2013. Geomorphic and human influence  
1081 on large-scale coastal change. *Geomorphology*, 199, 160-170.

1082 Hapke, C. J., Lentz, E. E., Gayes, P. T., McCoy, C. A., Hehre, R., Schwab, W. C., and Williams,  
1083 S. J., 2010. A review of sediment budget imbalances along Fire Island, New York: can  
1084 nearshore geologic framework and patterns of shoreline change explain the deficit? *Journal*  
1085 *of Coastal Research*, 510-522.

1086 Hapke, C. J., Plant, N. G., Henderson, R. E., Schwab, W. C., and Nelson, T. R., 2016. Decoupling  
1087 processes and scales of shoreline morphodynamics. *Marine geology*, 381, 42-53.

1088 ~~Hesp, P., 1988. Morphology, dynamics and internal stratification of some established foredunes in~~  
1089 ~~southeast Australia. *Sedimentary Geology*, 55(1-2), 17-41.~~

1090 Honeycutt, M. G., and Krantz, D. E., 2003. Influence of the geologic framework on spatial  
1091 variability in long-term shoreline change, Cape Henlopen to Rehoboth Beach, Delaware.  
1092 *Journal of Coastal Research*, 147-167.

1093 Hosking, J. R., 1981. Fractional differencing. *Biometrika*, 68(1), 165-176.

1094 Houser, C., Hapke, C., and Hamilton, S., 2008. Controls on coastal dune morphology, shoreline  
1095 erosion and barrier island response to extreme storms. *Geomorphology*, 100(3), 223-240.

1096 Houser, and Mathew, S., 2011. Alongshore variation in foredune height in response to transport  
1097 potential and sediment supply: South Padre Island, Texas. *Geomorphology*, 125(1), 62-72.

1098 Houser, C., 2012. Feedback between ridge and swale bathymetry and barrier island storm response  
1099 and transgression. *Geomorphology*, 173, 1-16.

1100 Houser, C., 2013. Alongshore variation in the morphology of coastal dunes: Implications for storm  
1101 response. *Geomorphology*, 199, 48-61.

1102 Houser, C., Wernette, P., Rentschlar, E., Jones, H., Hammond, B., and Trimble, S., 2015. Post-  
1103 storm beach and dune recovery: Implications for barrier island resilience.  
1104 *Geomorphology*, 234, 54-63.

1105 Hurst, H. E., 1951. Long-term storage capacity of reservoirs. *Trans. Amer. Soc. Civil Eng.*, 116,  
1106 770-808.

1107 Hyndman, R. J., 2015. Forecasting functions for time series and linear models. R package version  
1108 5.9., URL:<http://github.com/robjhyndman/forecast>.

1109 Hyndman, R. J., and Khandakar, Y., 2007. Automatic time series for forecasting: the forecast  
1110 package for R. Retrieved from

1111 Jol, H. M., Smith, D. G., and Meyers, R. A., 1996. Digital ground penetrating radar (GPR): a new  
1112 geophysical tool for coastal barrier research (Examples from the Atlantic, Gulf and Pacific  
1113 coasts, USA). *Journal of Coastal Research*, 960-968.

1114 Jol, H. M. (Ed.), 2008. *Ground penetrating radar theory and applications*. Elsevier.

1115 Kitchell, J. A., and Pena, D., 1984, Periodicity of extinctions in the geologic past: deterministic  
1116 versus stochastic explanations. *Science*, 226(4675), 689-692.

1117 Kraft, J., Belknap, D., McDonald, K., Maley, K., and Marx, P., 1982. Models of a shoreface-  
1118 nearshore marine transgression over estuarine and barrier systems and antecedent  
1119 topography of the Atlantic coast. Paper presented at the Geol. Soc. Am., Abstr. With  
1120 Programs.

1121 Lazarus, E., Ashton, A., Murray, A. B., Tebbens, S., and Burroughs, S., 2011. Cumulative versus  
1122 transient shoreline change: Dependencies on temporal and spatial scale. *Journal of*  
1123 *Geophysical Research: Earth Surface* (2003–2012), 116(F2).

1124 Lentz, E. E., and Hapke, C. J., 2011. Geologic framework influences on the geomorphology of an  
1125 anthropogenically modified barrier island: Assessment of dune/beach changes at Fire  
1126 Island, New York. *Geomorphology*, 126(1), 82-96.

1127 Lentz, E. E., Hapke, C. J., Stockdon, H. F., and Hehre, R. E., 2013. Improving understanding of  
1128 near-term barrier island evolution through multi-decadal assessment of morphologic  
1129 change. *Marine geology*, 337, 125-139.

1130 Linden, A., Adams, J. L., and Roberts, N., 2003. Evaluating disease management program  
1131 effectiveness: an introduction to time-series analysis. *Disease Management*, 6(4), 243-255.

**Formatted:** English (United States)

**Formatted:** Font: (Default) Times New Roman, 12 pt

**Formatted:** Font: (Default) Times New Roman, 12 pt, Not Italic

**Formatted:** Font: (Default) Times New Roman, 12 pt

**Formatted:** Font: (Default) Times New Roman, 12 pt, Not Italic

**Formatted:** Font: (Default) Times New Roman, 12 pt

**Formatted:** Font: 16 pt, English (United States)

**Formatted:** English (United States)

1132 Malamud, B. D., and Turcotte, D. L., 1999. Self-affine time series: I. Generation and  
1133 analyses. *Advances in Geophysics*, 40, 1-90.

1134 Mandelbrot, B. B., 1967. How long is the coast of Britain. *Science*, 156(3775), 636-638.

1135 Mandelbrot, B. B., and Taqqu, M. S., 1979. Robust R/S analysis of long run serial correlation:  
1136 IBM Thomas J. Watson Research Division.

1137 McNinch, J. E., 2004. Geologic control in the nearshore: shore-oblique sandbars and shoreline  
1138 erosional hotspots, Mid-Atlantic Bight, USA. *Marine geology*, 211(1), 121-141.

1139 Miselis, J. L., Buster, N. A., and Kindinger, J. L., 2014. Refining the link between the Holocene  
1140 development of the Mississippi River Delta and the geologic evolution of Cat Island, MS:  
1141 implications for delta-associated barrier islands. *Marine geology*, 355, 274-290.

1142 Miselis, J. L., and McNinch, J. E., 2006. Calculating shoreline erosion potential using nearshore  
1143 stratigraphy and sediment volume: Outer Banks, North Carolina. *Journal of Geophysical  
1144 Research: Earth Surface*, 111(F2).

1145 Morton, R. A., and Sallenger Jr, A. H., 2003. Morphological impacts of extreme storms on sandy  
1146 beaches and barriers. *Journal of Coastal Research*, 560-573.

1147 Murray, A. B., and Thieler, E. R., 2004. A new hypothesis and exploratory model for the formation  
1148 of large-scale inner-shelf sediment sorting and “rippled scour depressions”. *Continental  
1149 Shelf Research*, 24(3), 295-315.

1150 Neal, A., 2004. Ground-penetrating radar and its use in sedimentology: principles, problems and  
1151 progress. *Earth-science reviews*, 66(3), 261-330.

1152 Nobes, D. C., 1996. Troubled waters: Environmental applications of electrical and  
1153 electromagnetic methods. *Surveys in Geophysics*, 17(4), 393-454.

1154 NOAA., 2015a. National Hurricane Center. Data set accessed 29 April 2015 at  
1155 <http://www.nhc.noaa.gov/data/>.

1156 NOAA., 2015b. Tides and Currents. <https://tidesandcurrents.noaa.gov>, accessed 18 October, 2015.

1157 NOAA., 2017. Digital Coast. <https://coast.noaa.gov/digitalcoast/>, accessed 31 October, 2017.

1158 Nummedal, D., and Swift, D. J., 1987. Transgressive stratigraphy at sequence-bounding  
1159 unconformities: some principles derived from Holocene and Cretaceous examples.

1160 Otvos, E. G., and Giardino, M. J., 2004. Interlinked barrier chain and delta lobe development,  
1161 northern Gulf of Mexico. *Sedimentary Geology*, 169(1), 47-73.



1162 Plant, N. G., and Stockdon, H. F., 2012. Probabilistic prediction of barrier - island response to  
1163 hurricanes. Journal of Geophysical Research: Earth Surface, 117, F03015.

1164 Radliński, A., Radlińska, E., Agamalian, M., Wignall, G., Lindner, P., and Randl, O., 1999. Fractal  
1165 geometry of rocks. Physical Review Letters, 82(15), 3078.

1166 Riggs, S. R., Cleary, W. J., and Snyder, S. W., 1995. Influence of inherited geologic framework  
1167 on barrier shoreface morphology and dynamics Marine geology (Vol. 126, pp. 213-234).

1168 Rodriguez, A. B., Fassell, M. L., and Anderson, J. B., 2001. Variations in shoreface progradation  
1169 and ravinement along the Texas coast, Gulf of Mexico. Sedimentology, 48(4), 837-853.

1170 Sallenger Jr, A. H., 2000. Storm impact scale for barrier islands. Journal of Coastal Research, 16(3),  
1171 890-895.

1172 Samorodnitsky, G., 2007. Long range dependence. Foundations and Trends in Stochastic Systems,  
1173 1(3), 163-257.

1174 Santos, V. R., Porsani, J. L., Mendonça, C. A., Rodrigues, S. I., and DeBlasis, P. D., 2009.  
1175 Reduction of topography effect in inductive electromagnetic profiles: application on  
1176 coastal sambaqui (shell mound) archaeological site in Santa Catarina state, Brazil.  
1177 Journal of Archaeological Science, 36(10), 2089-2095.

1178 Schlager, W., 2004. Fractal nature of stratigraphic sequences. Geology, 32(3), 185-188.

1179 Schupp, C. A., McNinch, J. E., and List, J. H., 2006. Nearshore shore-oblique bars, gravel outcrops,  
1180 and their correlation to shoreline change. Marine geology, 233(1), 63-79.

1181 Schwab, W. C., Baldwin, W. E., Hapke, C. J., Lentz, E. E., Gayes, P. T., Denny, J. F., . . . Warner,  
1182 J. C., 2013. Geologic evidence for onshore sediment transport from the inner continental  
1183 shelf: Fire Island, New York. Journal of Coastal Research, 29(3), 526-544.

1184 Schwab, W. C., Thieler, E. R., Allen, J. R., Foster, D. S., Swift, B. A., and Denny, J. F., 2000.  
1185 Influence of inner-continental shelf geologic framework on the evolution and behavior of  
1186 the barrier-island system between Fire Island Inlet and Shinnecock Inlet, Long Island, New  
1187 York. Journal of Coastal Research, 408-422.

1188 Seijmonsbergen, A. C., Biewinga, D. T., and Pruijssers, A. P., 2004. A geophysical profile at the  
1189 foot of the Dutch coastal dunes near the former outlet of the 'Old Rhine'. Netherlands  
1190 Journal of Geosciences, 83(4), 287-291.

Formatted: Font: (Default) Times New Roman, 12 pt

Formatted: Font: 12 pt

Formatted: Font: (Default) Times New Roman, 12 pt

Formatted: Font: (Default) Times New Roman, 12 pt, Not Italic

Formatted: Font: (Default) Times New Roman, 12 pt

Formatted: Font: (Default) Times New Roman, 12 pt, Not Italic

Formatted: Font: (Default) Times New Roman, 12 pt

Formatted: Font: 16 pt

- 1191 Stewart, M. T., 1982. Evaluation of electromagnetic methods for rapid mapping of salt-water  
 1192 interfaces in coastal aquifers. *Groundwater*, 20(5), 538-545.
- 1193 Stone, G. W., Liu, B., Pepper, D. A., and Wang, P., 2004. The importance of extratropical and  
 1194 tropical cyclones on the short-term evolution of barrier islands along the northern Gulf of  
 1195 Mexico, USA. *Marine Geology*, 210(1), 63-78.
- 1196 Swarzenski, P. W., and Izbicki, J. A., 2009. Coastal groundwater dynamics off Santa Barbara,  
 1197 California: Combining geochemical tracers, electromagnetic seepmeters, and electrical  
 1198 resistivity. *Estuarine, Coastal and Shelf Science*, 83(1), 77-89.
- 1199 Talley, D. M., North, E. W., Juhl, A. R., Timothy, D. A., Conde, D., Jody, F., . . . Hall, C. J., 2003.  
 1200 Research challenges at the land–sea interface. *Estuarine, Coastal and Shelf Science*, 58(4),  
 1201 699-702.
- 1202 Tamura, T., 2012. Beach ridges and prograded beach deposits as palaeoenvironment  
 1203 records. *Earth-Science Reviews*, 114(3), 279-297.
- 1204 Taqqu, M. S., 2003. Fractional Brownian motion and long-range dependence. *Theory and*  
 1205 *applications of long-range dependence*, 5-38.
- 1206 Taqqu, M. S., Teverovsky, V., and Willinger, W., 1995. Estimators for long-range dependence: an  
 1207 empirical study. *Fractals*, 3(04), 785-798.
- 1208 Tebbens, S. F., Burroughs, S. M., and Nelson, E. E., 2002. Wavelet analysis of shoreline change  
 1209 on the Outer Banks of North Carolina: An example of complexity in the marine sciences.  
 1210 *Proceedings of the National Academy of Sciences*, 99(suppl 1), 2554-2560.
- 1211 Twichell, D. C., Flocks, J. G., Pendleton, E. A., and Baldwin, W. E., 2013. Geologic controls on  
 1212 regional and local erosion rates of three northern Gulf of Mexico barrier-island systems.  
 1213 *Journal of Coastal Research*, 63(sp1), 32-45.
- 1214 Veenstra, J., 2012. Persistence and Anti-persistence: Theory and Software. Ph.D. Thesis, Western  
 1215 University.
- 1216 Weise, B. R., and White, W. A., 1980. Padre Island National Seashore: A guide to the geology,  
 1217 natural environments, and history of a Texas barrier island (Vol. 17). Bureau of Economic  
 1218 Geology, University of Texas at Austin.
- 1219 Wernette, P., Houser, C., and Bishop, M. P., 2016. An automated approach for extracting Barrier  
 1220 Island morphology from digital elevation models. *Geomorphology*, 262, 1-7.

1221 Wernette, P., Houser, C., Weymer, B. A., Everett, M. E., Bishop, M. P., and Reece, B., 2018.  
1222 Influence of a spatially complex framework geology on barrier island  
1223 geomorphology. *Marine Geology*, 398, 151-162.

1224 Weymer, B. A., Everett, M. E., de Smet, T. S., and Houser, C., 2015a. Review of electromagnetic  
1225 induction for mapping barrier island framework geology. *Sedimentary Geology*, 321, 11-  
1226 24.

1227 Weymer, B. A., Everett, M. E., Houser, C., Wernette, P., and Barrineau, P., 2016. Differentiating  
1228 tidal and groundwater dynamics from barrier island framework geology: Testing the utility  
1229 of portable multi-frequency EMI profilers. *Geophysics*, 81, E347-E361.

1230 Weymer, B. A., Houser, C., and Giardino, J. R., 2015b. Poststorm Evolution of Beach-Dune  
1231 Morphology: Padre Island National Seashore, Texas. *Journal of Coastal Research*, 31(3),  
1232 634 – 644.

1233 Wilson, K. E., Adams, P. N., Hapke, C. J., Lentz, E. E., and Brenner, O., 2015. Application of  
1234 Bayesian Networks to hindcast barrier island morphodynamics. *Coastal Engineering*, 102,  
1235 30-43.

1236 Xu, T., Moore, I. D., and Gallant, J. C., 1993. Fractals, fractal dimensions and landscapes—a  
1237 review. *Geomorphology*, 8(4), 245-262.

1238  
1239  
1240  
1241  
1242  
1243  
1244  
1245  
1246  
1247  
1248  
1249  
1250

**Formatted:** Font: (Default) Times New Roman, 12 pt

**Formatted:** Font: (Default) Times New Roman, 12 pt

**Formatted:** Font: (Default) Times New Roman, 12 pt, Not Italic

**Formatted:** Font: (Default) Times New Roman, 12 pt

**Formatted:** Font: (Default) Times New Roman, 12 pt, Not Italic

**Formatted:** Font: (Default) Times New Roman, 12 pt

**Formatted:** Font: 16 pt

**Formatted:** Font: (Default) Times New Roman, 12 pt

**Formatted:** Font: (Default) Times New Roman, 12 pt

**Formatted:** Font: (Default) Times New Roman, 12 pt, Not Italic

**Formatted:** Font: (Default) Times New Roman, 12 pt

**Formatted:** Font: (Default) Times New Roman, 12 pt, Not Italic

**Formatted:** Font: (Default) Times New Roman, 12 pt

**Formatted:** Font: 16 pt

1251

1252

1253

1254 **Tables**

1255 **Table 1.** Comparison of residuals (RMSE) of each ARIMA model for the 100 km and 10 km  
1256 EMI surveys.

	<b>EMI (100 km)</b>	<b>EMI (10 km)</b>
<b>ARIMA (100)</b>	18.4	8.14
<b>ARIMA (001)</b>	49.7	41.1
<b>ARIMA (101)</b>	15.6	6.65
<b>ARIMA (202)</b>	40.6	7.31
<b>ARIMA (303)</b>	40.5	7.22
<b>ARIMA (404)</b>	40.3	7.22
<b>ARIMA (505)</b>	40.2	7.29
<b>ARIMA (111)</b>	15.8	5.72
<b>ARIMA (010)</b>	18.5	8.15
<b>ARIMA (0d0)</b>	15.5	5.55

1257

1258

1259

1260

1261

1262

1263

1264

1265

1266

1267

1268

1269

Formatted: Indent: Left: 0", First line: 0"

1270

1271

1272

1273 **Table 2.** Comparison of residuals (RMSE) of each ARIMA model for all spatial data series.

1274 Note that the residuals for each DEM metric correspond to the analysis performed at the regional

1275 scale (i.e., 100 km).

	<b>ARIMA</b> (100)	<b>ARIMA</b> (001)	<b>ARIMA</b> (101)	<b>ARIMA</b> (111)	<b>ARIMA</b> (010)	<b>ARIMA</b> (0d0)
<b>Beach width</b>	13.4	14.9	13.0	13.1	14.8	13.0
<b>Beach volume</b>	44.8	50.5	43.1	43.1	49.1	42.7
<b>Dune height</b>	0.7	0.8	0.7	0.7	0.8	0.7
<b>Dune volume</b>	60.6	63.9	59.7	59.2	69.03	58.9
<b>Island width</b>	138.4	253.2	121.3	121.1	140.8	120.9
<b>Island volume</b>	271.3	611.4	244.3	244.1	273.9	243.3

1276

1277

1278

1279

1280

1281

1282

1283

1284

1285

1286

1287

1288

1289

1290

1291

1292

1293

1294 **Table 3.** Summary table showing the computed *d* parameters that most appropriately model each  
1295 ARIMA (0*d*0) iteration (i.e., lowest RMSE).

Alongshore distance	Beach width	Beach volume	Dune height	Dune volume	Island width	Island volume	EMI $\sigma_a$
<b>“Regional”</b>							
<b>0-100 km</b>	0.38	0.42	0.34	0.32	0.13	~0.00	0.35
<b>“Intermediate”</b>							
<b>0-30 km</b>	~0.00	0.44	0.13	0.20	0.03	0.18	0.44
<b>30-60 km</b>	0.37	0.30	0.36	0.31	0.30	0.42	0.11
<b>60-100 km</b>	0.26	0.41	0.35	0.46	~0.00	0.50	0.49
<b>“Local”</b>							
<b>0-10 km</b>	0.41	0.39	0.20	0.21	0.09	0.18	0.36
<b>10-20 km</b>	0.30	0.42	0.20	0.26	0.37	~ 0.00	0.36
<b>20-30 km</b>	0.26	0.40	~ 0.00	~ 0.00	0.49	~ 0.00	~ 0.00
<b>30-40 km</b>	0.47	~ 0.00	0.41	0.25	0.29	0.28	~ 0.00
<b>40-50 km</b>	0.28	0.21	0.21	0.19	0.30	0.02	0.44
<b>50-60 km</b>	0.03	0.31	0.23	0.32	~ 0.00	0.33	0.48
<b>60-70 km</b>	0.16	0.37	0.29	0.34	~ 0.00	0.30	0.40
<b>70-80 km</b>	0.47	0.34	0.43	0.26	~ 0.00	0.42	0.49
<b>80-90 km</b>	0.27	0.19	0.42	0.39	0.01	0.02	~ 0.00
<b>90-100 km</b>	0.13	0.13	~ 0.00	0.06	0.44	0.47	0.41

1296

1297

1298

1299

1300

1301

1302

1303

1304

1305  
1306  
1307  
1308  
1309  
1310  
1311  
1312  
1313  
1314  
1315  
1316  
1317  
1318  
1319  
1320  
1321  
1322  
1323  
1324  
1325  
1326  
1327  
1328  
1329  
1330  
1331  
1332  
1333  
1334  
1335  
1336  
1337  
1338  
1339  
1340  
1341  
1342  
1343  
1344  
1345  
1346

**Figure Captions:**

**Figure 1.** Location map and DEM of the study area at Padre Island National Seashore (PAIS), Texas, USA. Elevations for the DEM are reported as meters above sea level (masl). Approximate locations of field images (red dots) from the northern (N), central (C), and southern (S) regions of the island showing alongshore differences in beach-dune morphology. Note: views are facing south for the central and southern locations, and the northern location view is to the north. Images taken in October, 2014.

**Figure 2.** 100 km (a) and 10 km (b) alongshore EMI surveys showing DEM's of study area and previously identified paleo-channel region by Fisk (1959). Channels are highlighted in red and green, where the green region indicates the location of the 10 km survey. 25 ft (7.6 m) contour intervals are highlighted with depths increasing from yellow to red and the center of the channels are represented by the black-dotted lines. For each survey, raw  $\sigma_a$  and zero-mean drift-corrected EMI responses are shown in grey and black, respectively. Tidal conditions during each EMI acquisition segment are shown below each panel. Low (lt) and falling tides (ft) are indicated by blue and light blue shades, respectively. High (ht) and rising tides (rt) are highlighted in red and light red, respectively.

**Figure 3.** Comparison of EMI  $\sigma_a$  responses from the 100 km survey with 100 MHz GPR data within one of the Fisk (1959) paleo-channels. The 800 m segment (A – A') crosses a smaller stream within the network of paleo-channels in the central zone of PAIS. The DOI of the 3 kHz EMI responses is outlined by the red box on the lower GPR radargram and the interpretation of the channel base (ravinement surface) is highlighted in yellow.

**Figure 4.** DEM metrics extracted from aerial LiDAR data. The sampling interval (step-size) for each data series is 10 m and the coordinates are matched with each EMI acquisition point. Each panel corresponds to a) beach width, b) beach volume, c) dune height, d) dune volume, e) island width, f) island volume, and g) EMI  $\sigma_a$ . The island is divided into three zones (red vertical lines) roughly indicating the locations within and outside the known paleo-channel region. A Savitzky-Golay smoothing filter was applied to all data series (LiDAR and EMI) using a moving window of  $n = 250$  to highlight the large-scale patterns in each signal.

**Figure 5.** Autocorrelations of  $\sigma_a$  for the 100 km (a) and 10 km EMI surveys (d). *R/S* analysis for the 100 km (b) and 10 km surveys (e). PSD plots for the 100 km (c) and 10 km surveys (f).

**Figure 6.** Examples of the worst (6a, 6c) and best (6b, 6d) fit ARIMA models for the 100 and 10 km EMI surveys. Model results are shown for the processed (drift-corrected)  $\sigma_a$  data. Residuals

1347 (RMSE) listed for each model gives the standard deviation of the model prediction error. For  
1348 each plot, original data is in red and fitted (model) data is in blue.

1349

1350 **Figure 7.** Example of the best fit ARIMA (0d0) models for each LiDAR-derived DEM metric: a)  
1351 beach width, b) beach volume, c) dune height, d) dune volume, e) island width, f) island volume.